Correlation function dependence of the scintillation behind a deep random phase screen

1977 J. Phys. A: Math. Gen. 10 1599

(http://iopscience.iop.org/0305-4470/10/9/016)

J. Phys. A: Math. Gen., Vol. 10, No. 9, 1977. Printed in Great Britain.

Correlation function dependence of the scintillation behind a deep random phase screen

E Jakeman and J G McWhirter

Royal Signals and Radar Establishment, St Andrews Road, Great Malvern, Worcestershire WR14 3PS, UK

Received 25 April 1977

Abstract. We investigate the role of the phase autocorrelation function in the generation of speckle, focusing and other scintillation effects produced when radiation is scattered by a deep random phase screen. New analytical formulae are obtained which reveal the mathematical origin of the observed physical phenomena, and these are supported by a range of numerically computed results.

1. Introduction

The characteristic pattern of bright and dark regions generated in the far field when coherent light is scattered by a rough surface and the changing intensity pattern produced on the floor of an illuminated swimming pool when the water surface is disturbed are, since the advent of the laser, equally familiar optical scattering phenomena. Neither phenomenon is peculiar to light scattering systems: both may be generated under the appropriate conditions when radiation of any frequency is scattered by a rough surface or phase screen, or propagates through a medium containing refractive index inhomogeneities.

The first mentioned pattern, usually referred to as 'speckle', is an interference effect produced by the coherent addition of independent contributions from different parts of the scatterer and is only visible when certain coherence criteria are satisfied by the incident radiation. The spatial structure of this type of pattern is statistically related to the effective size of the illuminated region contributing to the scattered field. If this region gives many randomly phased contributions, as is often the case, then the field is Gaussian distributed with zero mean by virtue of the central limit theorem.

The second phenomenon mentioned above is essentially a geometrical optics effect, arising from the focusing or lens-like behaviour of individual elements of the scatterer and is consequently visible in conditions of broad-band (e.g. white-light) illumination. The spatial structure of this type of intensity pattern is governed by the detailed nature of the scattering process; the statistics of the scattered field are non-Gaussian and the average contrast is typically greater than that of a speckle pattern.

Whereas the time dependence of a moving speckle pattern provides useful information regarding motion of or within a scattering system through techniques such as intensity fluctuation spectroscopy (Cummins and Pike 1974), its spatial structure can be used only to deduce the effective size of the region contributing to the field at the receiver. Moreover, in the Gaussian limit, its single interval statistics merely reflect the fact that this field is a sum of many independent randomly phased contributions. With

the important exception of applications such as the measurement of stellar diameters (Hanbury-Brown 1968) these latter properties have therefore been studied mainly in connection with the role of speckle as noise in measuring and detection systems (Dainty 1975).

It is evident from the above remarks that scattering systems which give rise to non-Gaussian effects such as focusing are of special interest for two reasons. Firstly, the statistical and spatial coherence properties of the scattered radiation carry more information about the scattering mechanism than in the case of Gaussian speckle. Secondly, high contrast fluctuations present a more severe limitation on the performance of measuring and detection systems than speckle noise. One scattering system which can, in principle, generate both speckle and non-Gaussian scintillation phenomena such as focusing, is the random phase screen. This is a scattering layer which introduces phase shifts which vary randomly across the wavefront of the incident radiation. It is a system of long-standing interest, providing a basis for theories of, for example, ionospheric scattering of radio waves (e.g. Bowhill 1961), stellar scintillation at optical frequencies (Briggs 1963, Taylor and Infosino 1975) and radio frequencies (e.g. Singleton 1970), rough surface scattering (Beckmann and Spizzichino 1963), dynamic scattering in liquid crystals (Jakeman and Pusey 1975) and optical propagation through the atmosphere (e.g. Prokhorov *et al* 1975). The mathematical formulation of the problem is straightforward and when the phase shifts introduced by the screen are equivalent to path differences which are short compared to the wavelength of the incident radiation (the 'weak' phase screen limit) solutions can be obtained by perturbation theory. This limit figures prominently in the literature and appears to be well understood. The opposite 'deep' phase screen limit has not received so much attention, being less amenable to both analytical and numerical methods of solution, but it is this limit in which contrasts in the intensity pattern can exceed the Gaussian value of unity.

The severity of the mathematical problem involved in the scattering of a plane wave by a random phase screen depends not only on the size of the phase shifts introduced but also on the model adopted for the statistical and coherence properties of the phase function at the screen. Thus, for simplicity, and want of a better model, joint Gaussian phase statistics are almost always assumed, whilst early workers in the field also generally adopted a Gaussian model for the phase correlation function (e.g. Mercier 1962). Until very recently calculations for an isotropic two-dimensional screen based on these assumptions had been carried out only for phase deviations equivalent to path differences of less than about half a wavelength of the incident radiation (Bramley and Young 1967) although numerical results have now been obtained for RMS phase shifts up to about 8 (Whale 1976). At the same time there have been various attempts to obtain analytical results valid for larger phase shifts in regions of special interest such as the focusing plane (Salpeter 1967). Most authors have only attempted to evaluate the field and intensity coherence functions of the scattered radiation and progress in understanding the mathematical structure of the problem has been made through analysis of the Fourier transforms of these quantities (Buckley 1971, Shishov 1971, Taylor and Infosino 1975). However, the relationship between the mathematics and the observed physical phenomena is not emphasised in this work. More recently 'power law' phase correlation functions have been used leading to models characterised by an 'effective' phase deviation which increases with propagation distance from the screen (Gochelashvily and Shishov 1975, Marians 1975, Rumsey 1975, Furuhama 1975).

These models seem to have arisen through the use of the Kolmogorov spectrum for turbulence in theories of atmospheric propagation. They achieve certain simplifica-

tions in the mathematics but can only accurately model limited portions of the true phase autocorrelation function since they behave in an unphysical way at both large and small spatial separations. Indeed the role of the phase autocorrelation function in determining the properties of the scattered radiation remains obscure. It is a particularly important aspect of the problem when the screen is deep, however, since the intensity pattern then becomes highly sensitive to the model adopted for the scatterer. Our own work (Jakeman and McWhirter 1976) has shown, for example, that a 'facet' model gives results which are qualitatively different from those obtained using a Gaussian model for the phase autocorrelation function.

Accordingly, in this paper we calculate the contrast and spatial coherence function of the intensity pattern behind a *deep* random phase screen by developing approximations in a 'real-space' formulation of the problem. These approximations both facilitate accurate numerical computation and allow the derivation of new analytical results in which the contributions of speckle and other scintillation effects such as focusing can easily be distinguished. We assume the phase function at the screen to be Gaussian distributed and consider three types of phase autocorrelation function, the present calculations being restricted to one-dimensional models for mathematical simplicity (two-dimensional results are presented elsewhere together with experimental data, Parry *et al* 1977). Unlike most previous work we examine scattering configurations in which only a limited area of the phase screen is illuminated and obtain results in both Fresnel and Fraunhofer limits with respect to this area. The last mentioned limit frequently occurs in laser light scattering experiments (Jakeman and Pusey 1975) but is also relevant to certain microwave scattering problems (Jakeman and Pusey 1976, Jakeman *et al* 1976).

In the next section we set up the mathematical formalism used throughout the paper and establish certain general properties of the solution to the phase screen scattering problem. The following sections concentrate on the deep phase screen limit. Scattering of a plane wave by a phase screen of infinite lateral extent (the Fresnel limit) is treated in § 3, where a number of new analytical and numerical results are obtained for the field and intensity coherence functions behind the screen using three different one-dimensional phase correlation functions. Section 4 similarly investigates the scattering of a focused beam into the Fraunhofer region and deals in addition with the angular dependence of the statistics. The principal steps in the mathematics are fully discussed in these two sections, more tedious aspects of the calculations being reserved for an appendix. The results and their implications are discussed in § 5 and the main conclusions to be drawn from the work are summarised in § 6.

2. Formulation of the problem and some general results

In this section we introduce the mathematical notation used in the remainder of the paper. We set down the formal solution of the scattering problem in a Huygens–Fresnel approximation and establish some general properties of this solution. Finally we discuss the three model phase autocorrelation functions to be used in the work.

2.1. Formal solution of the diffraction problem

The formal solution of the scattering problem illustrated in figure 1 is given, in a

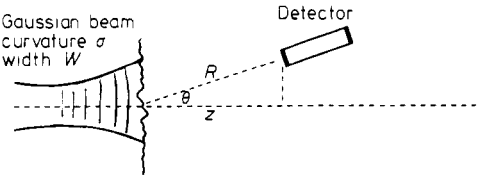

Figure 1. Scattering geometry.

Huygens–Fresnel approximation by (e.g. Jakeman and McWhirter 1976)

$$\mathscr{E}^+(\boldsymbol{R};t)=\frac{iE_0(1+\cos\theta)}{2\lambda R}\exp[i(kR-\omega t)] \times\int_{-\infty}^{\infty}d^2r'\exp[ik\kappa r'^2-ik\boldsymbol{r}'\cdot\boldsymbol{r}/R+i\phi(\boldsymbol{r}';t)-r'^2/W^2] \tag{2.1}$$

where

$$\kappa=\frac{1}{2}\left(\frac{1}{\sigma}+\frac{1}{R}\right),\qquad \cos\theta=\frac{z}{R},$$

$\mathscr{E}^+(\boldsymbol{R};t)$ is the positive frequency part of the scattered field or complex amplitude at the detection point $\boldsymbol{R}\equiv(r,z)\equiv(x,y,z)$ at time t, $\lambda(=2\pi/k)$ is the wavelength of the incident radiation, $\phi(\boldsymbol{r},t)$ the phase fluctuation introduced by the screen at the $z=0$ plane, and where, for mathematical convenience, we have assumed that the incident beam has a Gaussian amplitude profile of width W and radius of curvature σ. Time-dependent effects will not be considered in this paper and t will henceforth be dropped from the notation. The first-order (field) and second-order (intensity) coherence functions are defined in terms of the solution (2.1) by

$$|g^{(1)}(\boldsymbol{R},\boldsymbol{\Delta})|=\frac{|\langle\mathscr{E}^+(\boldsymbol{R})\mathscr{E}^-(\boldsymbol{R}+\boldsymbol{\Delta})\rangle|}{(\langle I(\boldsymbol{R})\rangle\langle I(\boldsymbol{R}+\boldsymbol{\Delta})\rangle)^{1/2}} \tag{2.2}$$

$$g^{(2)}(\boldsymbol{R},\boldsymbol{\Delta})=\frac{\langle I(\boldsymbol{R})I(\boldsymbol{R}+\boldsymbol{\Delta})\rangle}{\langle I(\boldsymbol{R})\rangle\langle I(\boldsymbol{R}+\boldsymbol{\Delta})\rangle} \tag{2.3}$$

where $\boldsymbol{\Delta}\equiv(\boldsymbol{\delta},\zeta)\equiv(\chi,\psi,\zeta)$ and the intensity I is the square of the envelope of the field:

$$I(\boldsymbol{R})=\mathscr{E}^+(\boldsymbol{R})\mathscr{E}^-(\boldsymbol{R}). \tag{2.4}$$

Expressions for (2.2) and (2.3) simplify in two useful limiting configurations:

$$k\kappa W^2\gg 1 \qquad \text{(the Fresnel limit)} \tag{2.5}$$

$$k\kappa W^2\ll 1 \qquad \text{(the Fraunhofer limit).} \tag{2.6}$$

We shall assume throughout §§ 3 and 4 that ϕ is joint-Gaussian distributed. If it is also stationary in a spatial sense with autocorrelation function

$$\rho(\boldsymbol{\delta})=\langle\phi(\boldsymbol{r})\phi(\boldsymbol{r}+\boldsymbol{\delta})\rangle/\langle\phi^2\rangle \tag{2.7}$$

then the transverse ($\zeta = 0$) spatial coherence functions are given in the Fresnel limit (2.5) by ($\langle \phi^2 \rangle = \phi_0^2$)

$$|g^{(1)}(z, \boldsymbol{\delta})| = \exp[-\phi_0^2(1-\rho(\boldsymbol{\delta}))] \tag{2.8}$$

$$g^{(2)}(z, \boldsymbol{\delta}) = \frac{1}{\lambda^2 z^2} \int_{-\infty}^{\infty} \mathrm{d}^2\boldsymbol{r}\, \mathrm{d}^2\boldsymbol{r}' \exp\left(-\phi_0^2 F(\boldsymbol{r}, \boldsymbol{r}') - \frac{\mathrm{i}k}{z}\boldsymbol{r}.(\boldsymbol{r}'+\boldsymbol{\delta})\right) \tag{2.9}$$

where

$$F(\boldsymbol{r}, \boldsymbol{r}') = 2 - 2\rho(\boldsymbol{r}) - 2\rho(\boldsymbol{r}') + \rho(\boldsymbol{r}+\boldsymbol{r}') + \rho(\boldsymbol{r}-\boldsymbol{r}'). \tag{2.10}$$

We have set $\boldsymbol{R} = (0, z)$ and $\sigma^{-1} = 0$ in (2.8) and (2.9) without loss of generality in order to clarify interpretation of the results.

Equations (2.8)–(2.10) provide the starting point for the analysis of § 3. A number of general properties of the coherence functions (2.8) and (2.9) may be established without assuming a model for $\rho(\boldsymbol{r})$, however. Equation (2.8) is in fact a special case of the more general result

$$|g^{(1)}(z, \boldsymbol{\delta})| = \langle \exp[\mathrm{i}(\phi(0) - \phi(\boldsymbol{\delta}))] \rangle \tag{2.11}$$

which can be established from (2.1) in the Fresnel limit (2.5) for a stationary random phase function with arbitrary distribution (Booker *et al* 1950).

Unlike the field coherence function, the intensity coherence function (2.9) approaches the value unity as $z \to 0$ since the intensity does not vary over the $z = 0$ plane:

$$g^{(2)}(0, \boldsymbol{\delta}) = 1. \tag{2.12}$$

By inspection, we also have

$$|g^{(1)}(z, \boldsymbol{\delta})| = g^{(2)}(z, \boldsymbol{\delta}) = 1 \qquad \text{if } \phi_0 = 0. \tag{2.13}$$

The last relation merely expresses the fact that, when no scattering screen is present, solution (2.1) describes (in the Fresnel region) the free propagation of a plane wave, i.e. the radiation remains coherent for all z.

Some interesting results can be derived in the limit of large z by making the linear transformation $\boldsymbol{r}' + \boldsymbol{\delta} \to \boldsymbol{r}'\sqrt{z}$, $\boldsymbol{r} \to \boldsymbol{r}\sqrt{z}$ in equations (2.9) and (2.10). Since, for a real stationary random process we must have

$$\lim_{r \to \infty} \rho(\boldsymbol{r}) = 0 \tag{2.14}$$

(i.e. all memory must be lost at sufficiently large sample separations), we can represent the asymptotic behaviour of $\rho(\boldsymbol{r}\sqrt{z})$ when z is large by the two-dimensional Kronecker delta:

$$\lim_{z \to \infty} \rho(\boldsymbol{r}\sqrt{z}) = \delta_{r,0} \begin{cases} = 1 & \text{for } \boldsymbol{r} \equiv (x, y) = (0, 0) \\ = 0 & \text{otherwise.} \end{cases} \tag{2.15}$$

It is not difficult to show that the exponential factor in (2.9) containing the function (2.10) is then given by ($X = \exp(-\phi_0^2\rho(\boldsymbol{\delta})) - 1$)

$$\begin{aligned} \lim_{z \to \infty} \exp(-\phi_0^2 F(\boldsymbol{r}\sqrt{z}, \boldsymbol{r}'\sqrt{z} - \boldsymbol{\delta})) \\ = \delta_{r,0} + \delta_{r',0} \exp[2\phi_0^2(\rho(\boldsymbol{\delta}) - 1)] + (1 - \delta_{r,0} - \delta_{r',0}) \exp(-2\phi_0^2) \\ + [\delta_{r,r'} + \delta_{r,-r'} - \delta_{r,0}\delta_{r',0} X(2X+3)/(X+1)^2] X \exp(-2\phi_0^2). \end{aligned} \tag{2.16}$$

Although the Kronecker delta's are non-zero over a set of points of measure zero, Dirac delta functions arising from the remaining exponential factor in (2.9) ensure finite contributions to the integral from all but the final group of terms appearing in (2.16). The result obtained is

$$\lim_{z\to\infty} g^{(2)}(z,\boldsymbol{\delta}) = 1 + |g^{(1)}(z,\boldsymbol{\delta})|^2 - \exp(-2\phi_0^2) \tag{2.17}$$

where $|g^{(1)}(z,\boldsymbol{\delta})|$ is given by (2.8).

Equation (2.17) is identical to a formula first derived by Mercier (1962) and reduces to the factorisation theorem for a zero mean circular complex Gaussian process when ϕ_0 is large. It appears to be a particular manifestation of a more general result which holds far from the scattering screen in the Fresnel limit provided that (2.14) is satisfied. This can be deduced using a simple intuitive argument with the help of figure 2 (see also Jakeman and Welford 1977). Because of (2.14), sufficiently far from the screen the scattered field is composed of many independent contributions of varying phase and amplitude. In the Fresnel limit these add with a systematic phase factor (the second term in the exponent on the right-hand side of (2.9)). When the screen introduces large random phase shifts this systematic factor will be unimportant by comparison with the large random changes of direction associated with each contribution. The scattered field is then the resultant of a two-dimensional random walk and will be Gaussian distributed with zero mean by virtue of the central limit theorem. When the phase screen is weak, the systematic phase factor imparts a spiral structure to the vector addition as illustrated in figure 2. The mean value of the resultant complex amplitude is

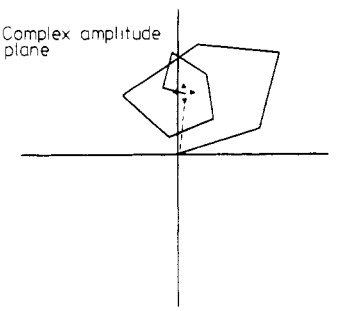

Figure 2. Vector addition of independent contributions to the scattered field in the Fresnel limit.

non-zero in this case. Since there are many contributions and many turns of the spiral, however, the real and imaginary part of this vector will again be Gaussian distributed, uncorrelated with equal variances (shown by arrows in figure 2). By analogy with the problem of homodyne detection in the presence of Gaussian noise (Rice 1944) the intensity of the resultant field will be Rice distributed (Re denotes real part):

$$\lim_{z\to\infty} P(I) = \frac{\exp[-(I+|\langle\mathscr{E}^+\rangle|^2)/2\,\mathrm{Var}(\mathrm{Re}\,\mathscr{E}^+)]}{2\,\mathrm{Var}(\mathrm{Re}\,\mathscr{E}^+)} I_0\left(\frac{|\langle\mathscr{E}^+\rangle|\sqrt{I}}{\mathrm{Var}(\mathrm{Re}\,\mathscr{E}^+)}\right) \tag{2.18}$$

with moments given by (e.g. Jakeman and Pike 1969)

$$\lim_{z\to\infty} \frac{\langle I^n\rangle}{\langle I\rangle^n} = n![2\,\mathrm{Var}(\mathrm{Re}\,\mathscr{E}^+)]^n L_n\left(\frac{-|\langle\mathscr{E}^+\rangle|^2}{2\,\mathrm{Var}(\mathrm{Re}\,\mathscr{E}^+)}\right). \tag{2.19}$$

In these expressions $\mathscr{E}^+$ is the asymptotic value of the complex amplitude at large distances from the screen, I_0 is the zeroth-order modified Bessel function of the first kind and L_n a Laguerre polynomial of degree n. The parameters entering (2.18) and (2.19) may be evaluated by observing that in the Fresnel region (2.5) the mean intensity is independent of distance from the screen. Normalising this quantity to unity, without loss of generality, and using the fact that the variances of the real and imaginary parts of $\mathscr{E}^+$ are equal we obtain

$$\mathrm{Var}(\mathrm{Re}\ \mathscr{E}^+) = \tfrac{1}{2}(1 - |\langle \mathscr{E}^+ \rangle|^2). \tag{2.20}$$

The remaining unknown parameter $|\langle \mathscr{E}^+ \rangle|$ can be evaluated directly from (2.1) in the Fresnel limit without further approximation. The result, after appropriate normalisation, is

$$|\langle \mathscr{E}^+ \rangle| = |\langle \exp(\mathrm{i}\phi) \rangle|. \tag{2.21}$$

Equations (2.18)–(2.21) provide a complete description of the first-order statistics of the intensity pattern far from the phase screen in the Fresnel limit (2.5). They are valid for arbitrary phase statistics and coherence properties provided only that $\phi(\boldsymbol{r})$ is spatially stationary and entirely random so that (2.14) is satisfied. The higher-order statistical properties of the intensity can also be obtained by analogy with the theory of homodyne detection in the presence of Gaussian noise (the moment generating function for the joint distribution of intensities is given in e.g. Jakeman 1970). Since the real and imaginary parts of $\mathscr{E}^+$ constitute a circular complex Gaussian process, the only new parameter entering into these properties is the first-order coherence function (2.2). It is not difficult to show, for example, that the intensity coherence function is given by

$$\lim_{z \to \infty} g^{(2)}(z, \boldsymbol{\delta}) = 1 + |g^{(1)}(z, \boldsymbol{\delta})|^2 - |\langle \mathscr{E}^+ \rangle|^4 \tag{2.22}$$

where $g^{(1)}(z, \boldsymbol{\delta})$ is defined by equation (2.11) and $|\langle \mathscr{E}^+ \rangle|$ by equation (2.21). Note that the results (2.18)–(2.22) reduce to those of Mercier (1962) when ϕ is Gaussian distributed.

Turning now to the Fraunhofer limit (2.6), we shall assume that the detection points are equidistant from the scattering region with $\boldsymbol{R}$, $\boldsymbol{R} + \boldsymbol{\Delta}$ and the x component of $\boldsymbol{R}$ in the same plane. Only the angular positions θ_1, θ_2 of the detection points will appear in (2.2) and (2.3) in this case and the un-normalised form of these coherence functions may, when ϕ is Gaussian distributed, be written

$$\langle \mathscr{E}^+(\theta_1) \mathscr{E}^-(\theta_2) \rangle = \frac{|E_0|^2 (1 + \cos\theta_1)(1 + \cos\theta_2)}{16\lambda^2 R^2} \int_{-\infty}^{\infty} \mathrm{d}^2 r' \, \mathrm{d}^2 r'' \times \exp\left(-\phi_0^2 (1 - \rho(r')) + \frac{\mathrm{i}k}{2} (x' U + x'' V) - \frac{r'^2 + r''^2}{2W^2} \right) \tag{2.23}$$

$$\langle I(\theta_1) I(\theta_2) \rangle = \pi W^2 |E_0|^4 (1 + \cos\theta_1)^2 (1 + \cos\theta_2)^2 / 16\lambda^4 R^4 \int_{-\infty}^{\infty} \mathrm{d}^2 r' \, \mathrm{d}^2 r'' \, \mathrm{d}^2 r''' \times \exp\left(-\phi_0^2 G(\boldsymbol{r}', \boldsymbol{r}'', \boldsymbol{r}''') + \mathrm{i}k (x'' U + x''' V) - \frac{r'^2 + r''^2 + r'''^2}{W^2} \right) \tag{2.24}$$

where

$$G(\boldsymbol{r}', \boldsymbol{r}'', \boldsymbol{r}''') = 2 - \rho(\boldsymbol{r}'' + \boldsymbol{r}''') - \rho(\boldsymbol{r}'' - \boldsymbol{r}''') - \rho(\boldsymbol{r}'' + \boldsymbol{r}') - \rho(\boldsymbol{r}'' - \boldsymbol{r}') + \rho(\boldsymbol{r}' + \boldsymbol{r}''') + \rho(\boldsymbol{r}' - \boldsymbol{r}''') \tag{2.25}$$

and

$$U = \sin\theta_1 + \sin\theta_2, \qquad V = \sin\theta_1 - \sin\theta_2. \tag{2.26}$$

The analysis of § 4 is based on equations (2.23)–(2.26). As in the Fresnel limit

$$|g^{(1)}(\theta_1, \theta_2)| = g^{(2)}(\theta_1, \theta_2) = 1 \qquad \text{if } \phi_0 = 0 \tag{2.27}$$

reflecting the fact that the solution (2.1) describes (in the Fraunhofer region) the propagation of a coherent beam of radiation of Gaussian amplitude profile far from its waist. Unlike the Fresnel limit it is difficult to obtain reduction of the formulae (2.23) and (2.24) in other more interesting situations because of the subtle interplay between the RMS phase deviation ϕ_0 and the effective number of contributions to the random walk problem which is dependent on W and the detailed behaviour of $\rho(\boldsymbol{r})$. This problem has been studied by Goodman (1975) and in more detail by Jakeman and Welford (1977) in the context of speckle in imaging systems. We note here only that if W is so large that there are many independent contributions to the scattered field (but still satisfies (2.6)), and ϕ_0 is also much greater than unity so that these contributions are randomly phased, then we might expect the scattered field to be Gaussian distributed with zero mean and the coherence functions to satisfy the factorisation relation

$$g^{(2)}(\theta_1, \theta_2) = 1 + |g^{(1)}(\theta_1, \theta_2)|^2. \tag{2.28}$$

We shall find later that in fact certain additional criteria must be satisfied for this result to be valid in the case of scattering by a random phase screen, in contrast to particle scattering situations frequently encountered in photon correlation spectroscopy, for example, when Gaussian statistics apply to a high degree of accuracy (Jakeman *et al* 1968).

2.2. Phase autocorrelation functions

In order to progress further with the evaluation of (2.8)–(2.19) or (2.23)–(2.24) in general situations a model must be assumed for the phase autocorrelation function (2.7). In the next two sections we investigate the following one-dimensional models:

(*a*) truncated parabolic

$$\rho(\boldsymbol{r}) = \begin{cases} 1 - x^2/\xi^2 & |x| < \xi \\ 0 & \text{otherwise} \end{cases} \tag{2.29}$$

(*b*) truncated linear

$$\rho(\boldsymbol{r}) = \begin{cases} 1 - |x|/\xi & |x| < \xi \\ 0 & \text{otherwise} \end{cases} \tag{2.30}$$

(*c*) Gaussian

$$\rho(\boldsymbol{r}) = \exp(-x^2/\xi^2). \tag{2.31}$$

The first two models, though characterised by an unphysical cut-off, do have the merit of satisfying (2.14). The truncated parabolic correlation function does not appear to

have been used explicitly in previous calculations although Fried (1965) has pointed out that *without the cut-off* this model is equivalent to a planar phase front with random tilt. The detected intensity in the Fresnel region is evidently constant in this case: in equation (2.9) $F(\boldsymbol{r}, \boldsymbol{r}')$ vanishes for all $\boldsymbol{r}, \boldsymbol{r}'$ so that $g^{(2)}(z, \boldsymbol{\delta}) = 1$. We shall find that the truncated form (2.29) leads to more interesting results and in fact corresponds to a one-dimensional analogue of the 'facet' model considered in our earlier publications.

Both the parabolic and linear correlation functions are, in the absence of the cut-off, special cases of the power law structure function $1-\rho(\boldsymbol{r}) = (ar)^{\alpha}$ investigated by a number of authors (Gochelashvily and Shishov 1975, Marians 1975, Rumsey 1975, Furuhama 1975) and lead to an intensity coherence function which depends on the single parameter $\phi_0^2(az/k)^{\alpha}$ in the Fresnel limit. Although truncation is essential in the case of the parabolic function (2.29) if non-trivial results are to be obtained (at least in the Fresnel limit), we shall establish that in the case of the linear correlation function (2.30) truncation has no effect on the calculations *in the deep phase screen limit* $\phi_0 \gg 1$. Our calculations are a one-dimensional analogue of those of Marians (1975) in this limit. It must be emphasised, however, that if ϕ_0 is not large truncation does have an effect on the predicted coherence properties because of the increased sensitivity of the results to the tail of the phase autocorrelation function. In particular, since an unmodified power law structure function fails to satisfy the physically reasonable memory condition (2.14), its use when ϕ_0 is not large may lead to incorrect results, at least in the asymptotic region far from the screen where we have shown (2.17) for example to be a direct consequence of this condition.

As we mentioned in the introduction, most early theoretical work on the phase screen scattering problem was based on the Gaussian phase autocorrelation function model (2.31) (e.g. Mercier 1962, Salpeter 1967, Bramley and Young 1967). Unlike the power law structure function, which derives from theories of turbulence, however, (2.31) appears as a rather *ad hoc* assumption. On the other hand, it does have the merit of satisfying (2.14) and also behaves in a physically reasonable way for small values of its argument. This is a particularly important property (again not shared with the unmodified power law structure function) when ϕ_0 is large because the behaviour of the coherence functions (2.2) and (2.3) is then largely governed by the behaviour of $\rho(\boldsymbol{r})$ near the origin. For this reason Buckley (1971) investigated the spectrum of intensity fluctuations and scintillation index in the deep phase screen limit $\phi_0 \gg 1$ using a 'multi-scale' phase autocorrelation function whose expansion near the origin is

$$\rho(\boldsymbol{r}) = 1 - \alpha r^2 + \beta r^4 - \gamma r^6 + \ldots . \tag{2.32}$$

Although his interpretation of the expansion coefficients appears to be non-unique the approach allowed him to derive many new analytical results and provided useful insight into the mathematical structure of the problem. In the present paper we consolidate this work by a combination of new numerical and analytical techniques and establish a connection between the various terms in our formulae and observed physical phenomena.

3. The Fresnel limit

In this section we evaluate (2.8) and (2.9) for the three correlation functions (2.29)–(2.31) assuming throughout that $\phi_0 \gg 1$. Approximations taking advantage of this inequality will be made on occasion and we shall imply by the statement 'to order $1/\phi_0$'

for example, that terms of this magnitude and smaller (i.e. higher powers of ϕ_0^{-1}) have been neglected. In order to clarify the mathematics we shall calculate the contrast or scintillation index

$$S = g^{(2)}(z, 0) - 1 \tag{3.1}$$

before evaluating $g^{(2)}(z, \Delta)$ in each case.

3.1. Truncated parabolic correlation function (model (a) of § 2.2)

For large ϕ_0 the field correlation function is given everywhere to order $\exp(-\phi_0^2)$ by

$$|g^{(1)}(z, \chi)| = \exp(-\phi_0^2 \chi^2/\xi^2) \tag{3.2}$$

where we have taken $\boldsymbol{\delta} \equiv (\chi, 0)$ in (2.8). The scintillation index defined by (3.1) and (2.9) may be evaluated by dividing the region of integration into areas according to the truncation of $\rho(\boldsymbol{r})$ as illustrated in figure 3 and using the symmetry in x and x'. Thus in

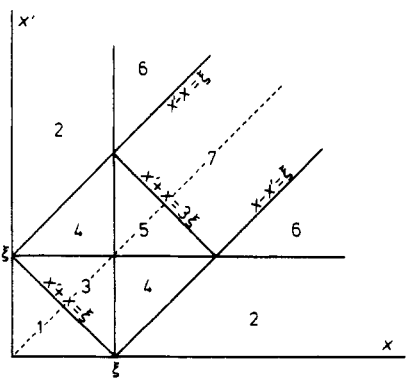

Figure 3. Regions of integration in the Fresnel limit.

region 1 $x + x' \leqslant \xi$, $|x - x'| < \xi$, $x' < \xi$, $x < \xi$ so that $F(x, x') \equiv 0$. The contribution to $g^{(2)}(z, 0)$ from this region may be evaluated in terms of Fresnel integrals (Abramowitz and Stegun 1965) by a transformation to sum and difference coordinates $a = x + x'$, $b = x - x'$:

$$I_1 = \frac{k}{4\pi z} \int_{-\xi}^{\xi} da \int_{-\xi}^{\xi} db \exp\left(\frac{ik}{4z}(a^2 - b^2)\right) = 2\left[C^2\left(\left(\frac{k\xi^2}{2\pi z}\right)^{1/2}\right) + S^2\left(\left(\frac{k\xi^2}{2\pi z}\right)^{1/2}\right)\right]. \tag{3.3}$$

In region 2 we have $x + x' > \xi$, $|x - x'| > \xi$ and either $x > \xi$, $x' < \xi$ or $x < \xi$, $x' > \xi$ so that $F(x, x') = 2x'^2/\xi^2$ or $2x^2/\xi^2$ respectively. The contributions from these two regions are clearly equal and the total is given by

$$I_2 = \frac{2k}{\pi z} \int_0^{\xi} dx' \int_{x'+\xi}^{\infty} dx \cos\left(\frac{k}{z} x x'\right) \exp\left(-\frac{2\phi_0^2 x'^2}{\xi^2}\right). \tag{3.4}$$

It is shown in appendix 1 that if $\phi_0 \gg 1$ and $k\xi^2/z\phi_0^2 \ll 1$ little error is incurred if the upper limit of the first integral is extended to infinity and x' set equal to zero in the lower

limit of the second integral. This leads to the result

$$I_2 = 2 - 2\,\mathrm{erf}\left(\frac{k\xi^2}{2z\phi_0\sqrt{2}}\right) \tag{3.5}$$

where $\mathrm{erf}(x)$ is the error function of argument x (Abramowitz and Stegun 1965). Contributions from the remaining areas illustrated in figure 3 are shown in appendix 1 to be negligible in this approximation and the scintillation index is therefore

$$S = 1 - 2\,\mathrm{erf}\left(\frac{k\xi^2}{2z\phi_0\sqrt{2}}\right) + 2\left[C^2\left(\left(\frac{k\xi^2}{2\pi z}\right)^{1/2}\right) + S^2\left(\left(\frac{k\xi^2}{2\pi z}\right)^{1/2}\right)\right]. \tag{3.6}$$

This quantity is plotted as a function of z for various values of ϕ_0^2 in figure 4.

The spatial coherence function (2.9) may be evaluated using a similar procedure but noting that there is in this case no symmetry about the line $x = x'$ in figure 3. The contribution from region 1 is again most simply expressed in terms of sum and difference coordinates:

$$\begin{aligned} I_1 &= \frac{k}{4\pi z}\int_{-\xi}^{\xi} \mathrm{d}a \int_{-\xi}^{\xi} \mathrm{d}b \exp\left(\frac{ik}{2z}\left[\tfrac{1}{2}(a^2 - b^2) + (a+b)\chi\right]\right) \\ &= \frac{1}{2}\left\{\left[C\left((\xi+\chi)\left(\frac{k}{2\pi z}\right)^{1/2}\right) + C\left((\xi-\chi)\left(\frac{k}{2\pi z}\right)^{1/2}\right)\right]^2\right. \\ &\quad \left. + \left[S\left((\xi+\chi)\left(\frac{k}{2\pi z}\right)^{1/2}\right) + S\left((\xi-\chi)\left(\frac{k}{2\pi z}\right)^{1/2}\right)\right]^2\right\}. \end{aligned} \tag{3.7}$$

The contribution from regions 2 is now the sum of two unequal integrals

$$\begin{aligned} I_2^{(1)} &= \frac{2k}{\pi z}\int_0^{\xi} \mathrm{d}x' \int_{x'+\xi}^{\infty} \mathrm{d}x \cos\left(\frac{kxx'}{z}\right)\cos\left(\frac{kx\chi}{z}\right)\exp\left(-\frac{2\phi_0^2 x'^2}{\xi^2}\right) \\ I_2^{(2)} &= \frac{2k}{\pi z}\int_0^{\xi} \mathrm{d}x \int_{x+\xi}^{\infty} \mathrm{d}x' \cos\left(\frac{kxx'}{z}\right)\cos\left(\frac{kx\chi}{z}\right)\exp\left(-\frac{2\phi_0^2 x^2}{\xi^2}\right). \end{aligned} \tag{3.8}$$

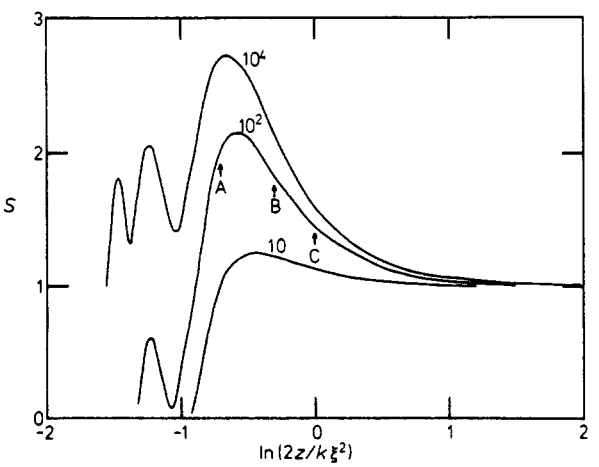

Figure 4. Scintillation index against distance from the screen for the values of ϕ_0^2 shown: truncated parabolic phase autocorrelation function, Fresnel limit. The height of the peak is already nearing saturation when $\phi_0^2 = 10^4$.

As before, provided $\phi_0 \gg 1$, the upper limit of the first integral in each of (3.8) may be extended to infinity and the lower limit of the second set equal to ξ without incurring serious error. To order $1/\phi_0$ we then obtain (Re denotes real part)

$$I_2^{(1)} = \exp\left(-\frac{2\phi_0^2\chi^2}{\xi^2}\right)\left[1 - \text{Re erf}\left(\frac{k\xi^2}{2z\phi_0\sqrt{2}} + \frac{i\chi\phi_0\sqrt{2}}{\xi}\right)\right]$$
$$I_2^{(2)} = 1 - \tfrac{1}{2}\left[\text{erf}\left(\frac{k\xi(\xi+\chi)}{2z\phi_0\sqrt{2}}\right) + \text{erf}\left(\frac{k\xi(\xi-\chi)}{2z\phi_0\sqrt{2}}\right)\right] \tag{3.9}$$

and finally, since the contributions from all other regions are negligible to this order

$$g^{(2)}(z,\chi) = 1 - \frac{1}{2}\left[\text{erf}\left(\frac{k\xi(\xi+\chi)}{2z\phi_0\sqrt{2}}\right) + \text{erf}\left(\frac{k\xi(\xi-\chi)}{2z\phi_0\sqrt{2}}\right)\right]$$
$$+ |g^{(1)}(z,\chi)|^2\left[1 - \text{Re erf}\left(\frac{k\xi^2}{2z\phi_0\sqrt{2}} + \frac{i\chi\phi_0\sqrt{2}}{\xi}\right)\right]$$
$$+ \frac{1}{2}\left\{\left[C\left((\xi+\chi)\left(\frac{k}{2\pi z}\right)^{1/2}\right) + C\left((\xi-\chi)\left(\frac{k}{2\pi z}\right)^{1/2}\right)\right]^2\right.$$
$$\left. + \left[S\left((\xi+\chi)\left(\frac{k}{2\pi z}\right)^{1/2}\right) + S\left((\xi-\chi)\left(\frac{k}{2\pi z}\right)^{1/2}\right)\right]^2\right\}. \tag{3.10}$$

This formula is plotted as a function of χ for $\phi_0^2 = 100$ and various values of $2z/k\xi^2$ in figure 5. ($|g^{(1)}(z,\chi)|$ is given by (3.2).)

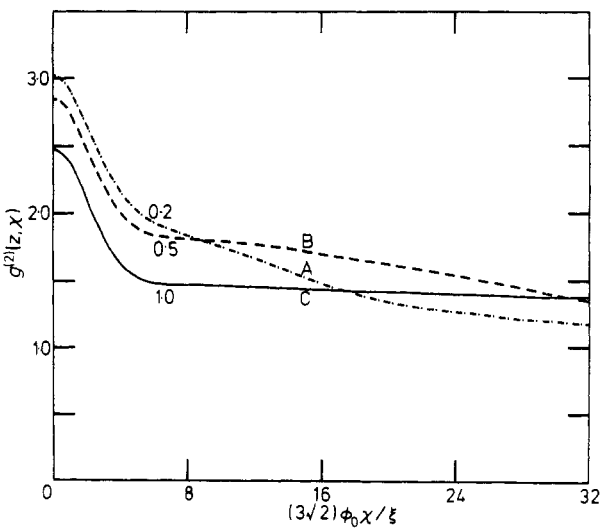

Figure 5. Spatial coherence function of intensities for values of $2z/k\xi^2$ indicated by arrows in figure 4: truncated parabolic phase autocorrelation function, Fresnel limit $\phi_0^2 = 100$.

3.2. Truncated linear correlation function (model (b) of § 2.2)

In this case the field correlation function is given to order $\exp(-\phi_0^2)$ by ($\boldsymbol{\delta} \equiv (\chi, 0)$)

$$|g^{(1)}(z,\chi)| = \exp(-\phi_0^2|\chi|\xi). \tag{3.11}$$

The scintillation index may again be expressed as the sum of several contributions corresponding to the areas illustrated in figure 3. In area 1 $F(x, x') = 2x/\xi$ if $x < x'$ or $2x'/\xi$ of $x > x'$ and the contribution from this region of integration is thus

$$I_1 = \frac{4k}{\pi z}\int_0^{\xi/2} dx' \int_{x'}^{\xi - x'} dx \exp\left(-\frac{2\phi_0^2 x'}{\xi}\right)\cos\left(\frac{kxx'}{z}\right). \tag{3.12}$$

It is shown in appendix 2 that extending the limit of the first integral to infinity incurs an error of order $\exp(-\phi_0^2)$. In region 2 $F(x, x') = 2x/\xi$ if $x < x'$ and $2x'/\xi$ if $x > x'$ so that the contribution from this region is

$$I_2 = \frac{4k}{\pi z}\int_0^{\xi} dx' \int_{x'+\xi}^{\infty} dx \cos\left(\frac{kxx'}{z}\right)\exp\left(-\frac{2\phi_0^2 x'}{\xi}\right). \tag{3.13}$$

Again the upper limit of the first integral may be extended to infinity (appendix 2) and combining I_1 with I_2 we obtain

$$\begin{aligned} I_1 + I_2 = {} & \frac{4k}{\pi z}\int_0^{\infty} dx' \int_{x'}^{\infty} dx \cos\left(\frac{kxx'}{z}\right)\exp\left(-\frac{2\phi_0^2 x'}{\xi}\right) \\ & -\frac{8}{\pi}\int_0^{\infty}\frac{dx'}{x'}\cos\left(\frac{k\xi x'}{z}\right)\sin\left(\frac{kx'^2}{z}\right)\exp\left(-\frac{2\phi_0^2 x'}{\xi}\right). \end{aligned} \tag{3.14}$$

It is shown in appendix 2 that the last integral in (3.14) may be neglected if $\phi_0 \gg 1$, and that contributions from the remaining areas of figure 3 are also negligible in this limit. From (3.14) we then have

$$S + 1 = \frac{4k}{\pi z}\int_0^{\infty} dx' \int_{x'}^{\infty} dx \cos\left(\frac{kxx'}{z}\right)\exp\left(-\frac{2\phi_0^2 x'}{\xi}\right). \tag{3.15}$$

The right-hand side may be expressed in terms of Fresnel integrals and the scintillation index is then given by

$$S = 1 - 2\left\{\left[\frac{1}{2} - C\left(\left(\frac{2z\phi_0^4}{\pi k\xi^2}\right)^{1/2}\right)\right] + \left[\frac{1}{2} - S\left(\left(\frac{2z\phi_0^4}{\pi k\xi^2}\right)^{1/2}\right)\right]^2\right\}. \tag{3.16}$$

A plot of this function is shown in figure 6.

The spatial coherence function may be evaluated following a similar procedure.

As in case (*a*) (§ 3.1) it is necessary to further subdivide the regions of integration illustrated in figure 3 according as x is less than or greater than x' because of loss of symmetry when $\chi \neq 0$. The contribution from region 1 is the sum of the integrals

$$\begin{aligned} I_1^{(1)} &= \frac{2k}{\pi z}\int_0^{\xi/2} dx' \int_{x'}^{\xi - x'} dx \cos\left(\frac{kxx'}{z}\right)\cos\left(\frac{kx'\chi}{z}\right)\exp\left(-\frac{2\phi_0^2 x'}{\xi}\right) \\ I_1^{(2)} &= \frac{2k}{\pi z}\int_0^{\xi/2} dx' \int_{x'}^{\xi - x'} dx \cos\left(\frac{kxx'}{z}\right)\cos\left(\frac{kx\chi}{z}\right)\exp\left(-\frac{2\phi_0^2 x'}{\xi}\right) \end{aligned} \tag{3.17}$$

whilst the contribution from region 2 is the sum of the integrals

$$\begin{aligned} I_2^{(1)} &= \frac{2k}{\pi z}\int_0^{\xi} dx' \int_{x'+\xi}^{\infty} dx \cos\left(\frac{kxx'}{z}\right)\cos\left(\frac{kx'\chi}{z}\right)\exp\left(-\frac{2\phi_0^2 x'}{\xi}\right) \\ I_2^{(2)} &= \frac{2k}{\pi z}\int_0^{\xi} dx' \int_{x'+\xi}^{\infty} dx \cos\left(\frac{kxx'}{z}\right)\cos\left(\frac{kx\chi}{z}\right)\exp\left(-\frac{2\phi_0^2 x'}{\xi}\right). \end{aligned} \tag{3.18}$$

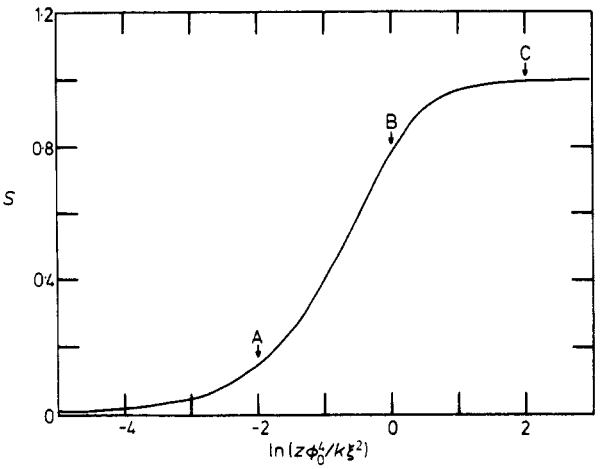

Figure 6. Scintillation index against distance from the screen: truncated linear phase autocorrelation function, Fresnel limit.

The four sets of integrals (3.17)–(3.18) may be evaluated to the same order of approximation as before by extending the upper limit of the first integral in each expression to infinity and combining $I_1^{(1)}$ with $I_2^{(1)}$ and $I_1^{(2)}$ with $I_2^{(2)}$ as described in the derivation of equation (3.16). The results are most simply expressed in terms of the spatial frequency ω:

$$g^{(2)}(z,\chi)=1+|g^{(1)}(z,\chi)|^2-\frac{4\phi_0^2}{\pi\xi}\int_0^\infty d\omega\cos(\omega\chi)\frac{\exp(-2\phi_0^2z\omega/k\xi)}{\omega[\omega^2+(2\phi_0^2/\xi)^2]}$$
$$\times\left[\frac{2\phi_0^2}{\xi}\sin\left(\frac{\omega^2z}{k}\right)+\omega\cos\left(\frac{\omega^2z}{k}\right)\right] \tag{3.19}$$

where $|g^{(1)}(z,\chi)|$ is given by (3.11). Fourier transformation of this quantity gives the frequency spectrum in terms of elementary functions:

$$S^{(2)}(z,\omega)=\pi\delta(\omega)+\frac{2\phi_0^2/\xi}{\omega^2+(2\phi_0^2/\xi)^2}$$
$$\times\left\{1-\frac{\exp(2\phi_0^2z\omega/k\xi)}{\omega}\left[\frac{2\phi_0^2}{\xi}\sin\left(\frac{\omega^2z}{k}\right)+\omega\cos\left(\frac{\omega^2z}{k}\right)\right]\right\}. \tag{3.20}$$

Formula (3.19) depends only on $\phi_0^2|\chi|/\xi$ and the parameter $\phi_0^4z/k\xi^2$ and is plotted in figure 7. The frequency spectrum (3.20) is also shown in figure 8 in order to allow comparison with the work of previous authors.

3.3. Gaussian correlation function (model (c) of § 2.2)

When ϕ_0 is large the field correlation function (2.8) for this type of correlation function is given to order $\exp(-\phi_0^2)$ by ($\boldsymbol{\delta}=(\chi,0)$)

$$|g^{(1)}(z,\chi)|=\exp(-\phi_0^2\chi^2/\xi^2) \tag{3.21}$$

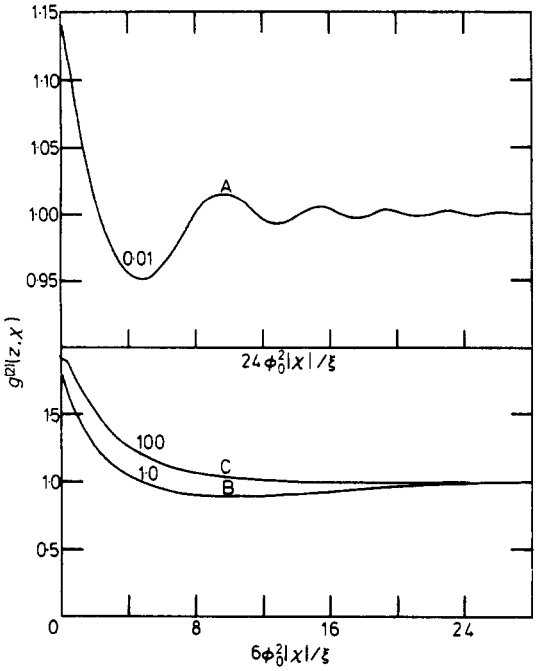

Figure 7. Spatial coherence function of intensities for values of $z\phi_0^4/k\xi^2$ indicated by arrows in figure 6: truncated linear phase autocorrelation function, Fresnel limit.

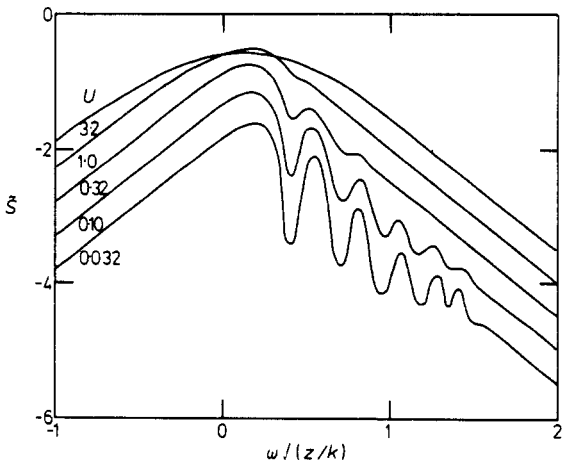

Figure 8. Spectrum of intensity fluctuations $\tilde{S} = \ln(\sqrt{(k/z)}S^{(2)}(\omega))$ for truncated linear phase autocorrelation function in the Fresnel limit, plotted for comparison with the results of Marians (1975). The parameter $U = 2\phi_0^2\sqrt{(z/k\xi^2)}$ relates each curve to a position on the scintillation plot, figure 6.

which is identical to the result (3.2) obtained in the case of the truncated parabolic function (case (*a*), § 3.1). Evaluation of the scintillation index is not so straightforward as in the preceding examples since figure 3 is no longer relevant in the absence of truncation. The main contributions to S still come from regions near the $x - x'$ axes,

however. More precisely they arise from regions where the function

$$F(x, x') = 2 - 2\exp(-x^2/\xi^2) - 2\exp(-x'^2/\xi^2) + \exp[-(x+x')^2/\xi^2] + \exp[-(x-x')^2/\xi^2] \tag{3.22}$$

is minimum. It is readily shown that the derivatives $\partial F/\partial x$ and $\partial F/\partial x'$ both vanish for all x' if $x = 0$ and also for all x if $x' = 0$, i.e. along the axes. Taking advantage of the symmetry in (2.9) we see that the scintillation index can be expressed in terms of an integral over the lower half quadrant shown in figure 3. In this region we approximate $F(x, x')$ by the second-order Taylor expansion

$$F(x, x') \simeq F(x, 0) + \frac{x'^2}{2}\frac{d^2}{dx'^2}F(x, x')\Big|_{x'=0} \tag{3.23}$$

so that

$$S + 1 \simeq \frac{4k}{\pi z}\int_0^\infty dx \int_0^x dx' \cos\left(\frac{kxx'}{z}\right) \exp\left\{-\frac{2\phi_0^2 x'^2}{\xi^2}\left[1 - \exp\left(-\frac{x^2}{\xi^2}\right)\left(1 - \frac{2x^2}{\xi^2}\right)\right]\right\}. \tag{3.24}$$

This approximate formula is extremely accurate even for moderate values of ϕ_0 and greatly facilitates numerical computation of the scintillation index. Plots of S against normalised distance from the screen are displayed in figure 9 for various values of ϕ_0^2 together with numerical results obtained by previous authors.

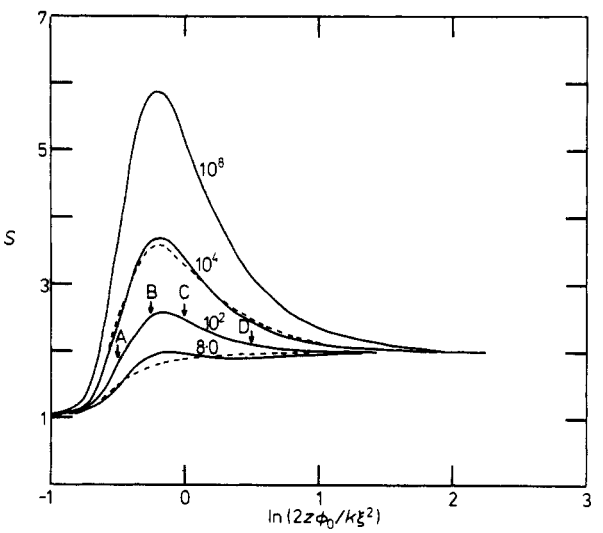

Figure 9. Scintillation index against distance from the screen for the values of ϕ_0^2 shown: Gaussian phase autocorrelation function, Fresnel limit. The lowest curve ($\phi_0^2 = 8$) is indistinguishable from the result of Whale (1973). The broken curves correspond to the analytical formula (3.34) of the text.

(3.24) is relatively insensitive to the function of x appearing in the exponent of the integral. In order to proceed further, therefore, we model this function as follows

$$\exp\left(-\frac{x^2}{\xi^2}\right)\left(1 - \frac{2x^2}{\xi^2}\right) \simeq \begin{cases} 1 - 3x^2/\xi^2 & x < \xi/\sqrt{3} \\ 0 & \text{otherwise} \end{cases} \tag{3.25}$$

so that

$$S+1=\frac{4k}{\pi z}\int_0^{\xi/\sqrt{3}}dx\int_0^x dx'\cos\left(\frac{kxx'}{z}\right)\exp\left(-\frac{6\phi_0^2x^2x'^2}{\xi^4}\right)$$
$$+\frac{4k}{\pi z}\int_{\xi/\sqrt{3}}^{\infty}dx\int_0^x dx'\cos\left(\frac{kxx'}{z}\right)\exp\left(-\frac{2\phi_0^2x'^2}{\xi^2}\right). \tag{3.26}$$

The substitution $x'=t/x$ in the first integral followed by an integration over t by parts reduces it to the form

$$I_1=-\frac{2k}{\pi z}\int_0^{\infty}dx\,\ln\left(\frac{3x}{\xi^2}\right)\cos\left(\frac{kx}{z}\right)\exp\left(-\frac{6\phi_0^2x^2}{\xi^4}\right) \tag{3.27}$$

where the upper limit has been extended to infinity incurring an error of order $\exp(-\phi_0^2)$ only. (3.27) is evaluated in appendix 3 to give

$$I_1=\frac{q}{\sqrt{\pi}}\exp(-q^2)\left[\ln\left(\frac{8\gamma\phi_0^2}{3}\right)+\pi\,\mathrm{erfi}(q)-R(q)\right]. \tag{3.28}$$

Here $\mathrm{erfi}(q)$ is an error function of imaginary argument (Erdélyi 1953):

$$\mathrm{erfi}(q)=\frac{2}{\sqrt{\pi}}\int_0^q dx\,\exp(x^2), \tag{3.29}$$

whilst

$$R(q)=4\int_0^q\exp(x^2)\,dx\int_x^{\infty}\exp(-y^2)\,dy \tag{3.30}$$

satisfies the inequality

$$2\ln\left(\frac{q+\sqrt{(q^2+2)}}{\sqrt{2}}\right)+\frac{2q}{q+\sqrt{(q+2)}}<R(q)\leqslant 2\ln\left(\frac{q+\sqrt{(q^2+4/\pi)}}{2/\sqrt{\pi}}\right)+\frac{2q}{q+\sqrt{(q^2+4/\pi)}}. \tag{3.31}$$

$\gamma=e^C\simeq 1{\cdot}781$ where C is the Euler–Mascheroni constant, and, for compactness of notation, we have introduced the dimensionless reciprocal length parameter

$$q=k\xi^2/2z\phi_0\sqrt{6}. \tag{3.32}$$

The second double integral appearing in (3.26) can be evaluated by noting that an error of only $\exp(-\phi_0^2)$ is introduced by extending the upper limit x to infinity. We obtain

$$I_2=2\,\mathrm{erfc}(q)=2[1-\mathrm{erf}(q)] \tag{3.33}$$

and finally

$$S=1-2\,\mathrm{erf}(q)+\frac{q}{\sqrt{\pi}}\exp(-q^2)\left[\ln\left(\frac{8\gamma\phi_0^2}{3}\right)+\pi\,\mathrm{erfi}(q)-R(q)\right]. \tag{3.34}$$

This result is compared with results obtained by direct numerical evaluation of (3.24) in figure 9.

Numerical computation of the spatial coherence function (2.9) is also greatly facilitated by using the Taylor expansion approach described above. Because of the

asymmetry introduced with respect to the line $x = x'$ in figure 3 the two half quadrants must be considered separately. We obtain after some manipulation:

$$g^{(2)}(z,\chi)=\frac{2k}{\pi z}\int_0^\infty dx\int_0^x dx'\left[\cos\left(\frac{kx\chi}{z}\right)+\cos\left(\frac{kx'\chi}{z}\right)\right]\cos\left(\frac{kxx'}{z}\right)$$
$$\times\exp\left\{-\frac{2\phi_0 x'^2}{\xi^2}\left[1-\exp\left(-\frac{x^2}{\xi^2}\right)\left(1-\frac{2x^2}{\xi^2}\right)\right]\right\}. \tag{3.35}$$

This quantity is plotted as a function of χ for $\phi_0^2 = 100$ and various values of $2z/k\xi^2$ in figure 10. To proceed further analytically we again use the model (3.25):

$$g^{(2)}(z,\chi)=\frac{2k}{\pi z}\int_0^{\xi/\sqrt{3}} dx\int_0^x dx'\left[\cos\left(\frac{kx\chi}{z}\right)+\cos\left(\frac{kx'\chi}{z}\right)\right]\cos\left(\frac{kxx'}{z}\right)\exp\left(-\frac{6\phi_0^2x^2x'^2}{\xi^4}\right)$$
$$+\frac{2k}{\pi z}\int_{\xi/\sqrt{3}}^\infty dx\int_0^x dx'\left[\cos\left(\frac{kx\chi}{z}\right)+\cos\left(\frac{kx'\chi}{z}\right)\right]\cos\left(\frac{kxx'}{z}\right)\exp\left(-\frac{2\phi_0^2x'^2}{\xi^2}\right). \tag{3.36}$$

These integrals are evaluated to the usual order of approximation in appendix 3 but the resulting expressions are lengthy and will not be presented here. An instructive limiting situation in which relatively simple but useful formulae may be obtained occurs when q

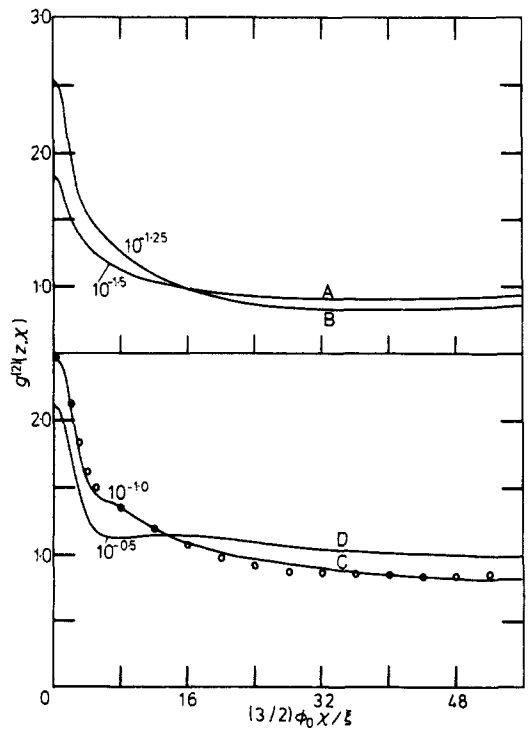

Figure 10. Spatial coherence function of intensities for values of $2z/k\xi^2$ indicated by arrows in figure 9: Gaussian phase autocorrelation function, Fresnel limit, $\phi_0^2 = 100$. The open circles correspond to the analytical formula (3.37) of the text. All curves saturate at unity for sufficiently large values of χ.

(equation (3.32)) is small. Retaining only the terms from (3.36) which are significant in this limit we obtain (appendix 3)

$$g^{(2)}(z,\chi)=1+|g^{(1)}(z,\chi)|^2-\frac{2q}{\sqrt{\pi}}\left[\frac{\sin(k\xi\chi/z\sqrt{3})}{k\xi\chi/z\sqrt{3}}+\exp\left(-\frac{k^2\xi^2\chi^2}{8z^2\phi_0^2}\right)\right]$$
$$+\frac{2q}{\sqrt{\pi}}\left[\mathrm{Ci}\left(\frac{k\xi\chi}{z\sqrt{3}}\right)+\frac{1}{2}\mathrm{E}_1\left(\frac{k^2\xi^2\chi^2}{8z^2\phi_0^2}\right)\right] \tag{3.37}$$

where $\mathrm{E}_1(x)$ and $\mathrm{Ci}(y)$ are the exponential and cosine integrals respectively (Erdélyi 1953) and $|g^{(1)}(z,\chi)|$ is given by equation (3.21). A comparison of this formula with numerically computed results is given in figure 10.

4. The Fraunhofer limit

In this section we evaluate the field coherence function, scintillation index and intensity coherence function for the three one-dimensional phase correlation functions (2.29)–(2.31) in the Fraunhofer limit (2.6). It will again be assumed throughout that $\phi_0 \gg 1$ and further, that $\xi < W$. In order to obtain analytical results in some cases we shall consider only the limit $\xi \ll W$. This condition, though more restrictive than $\xi < W$ is nevertheless a commonly occurring situation in practice.

4.1. Truncated parabolic correlation function (model (a) of § 2.2)

Neglecting the cut-off at $x'=\xi$ in the phase correlation function appearing on the right-hand side of (2.23) incurs an error of only $\exp(-\phi_0^2)$ and the integral may be evaluated to this order of approximation to give

$$\langle \mathscr{E}^+(\theta_1)\mathscr{E}^-(\theta_2)\rangle=\frac{|E_0|^2(1+\cos\theta_1)(1+\cos\theta_2)W^3\xi\pi^2}{4\lambda^2R^2\phi_0\sqrt{2}}\exp\left(-\frac{k^2V^2W^2}{8}\right)$$
$$\times\exp\left(-\frac{k^2U^2\xi^2}{16\phi_0^2}\right) \tag{4.1}$$

so that the mean intensity and field coherence function are given by

$$\langle I(\theta)\rangle=\frac{|E_0|^2(1+\cos\theta)^2W^3\xi\pi^2}{4\lambda^2R^2\phi_0\sqrt{2}}\exp\left(-\frac{k^2\xi^2\sin^2\theta}{4\phi_0^2}\right) \tag{4.2}$$

and

$$g^{(1)}(\theta_1,\theta_2)=\exp\left(-\frac{k^2V^2W^2}{8}\right). \tag{4.3}$$

The scintillation index is obtained from (2.24) with $V=0$, i.e. $\theta_1=\theta_2=\theta$. Evaluation of the integrals is accomplished by dividing up the region of integration according to the truncation of the phase correlation function. Since this is a function only of the x coordinate (2.24) reduces to a volume integral and the symmetries of the integrals imply that only the first octant need be considered. Inspection of (2.25) indicates that the main contributions to the integral come from regions near the $x'-x'''$ plane when $\phi_0 \gg 1$. Note, moreover, than when $x''\equiv 0$ (2.25) reduces to (2.10), i.e. $G(r',0,r''')\equiv F(r',r''')$. Thus we expect the principle contributions to (2.24) to originate from regions

near the x' and x''' axes as in figure 3. These regions are sketched in figure 11. The central region is a tetrahedron whose edges coincide with the axes and the lines $x'+x''=x'+x'''=x''+x'''=\xi$. Within this region $G(x', x'', x''')=4x''^2/\xi^2$ and its contribution to the integral (2.24) is

$$I_1 = A(\theta, \theta)\int_0^{\xi} dx'' \int_0^{\xi-x''} dx''' \int_0^{\xi-x''-x'''} dx' \cos(2kx'' \sin\theta) \times \exp\left[-\left(\frac{x'^2+x''^2+x'''^2}{W^2}+\frac{4\phi_0^2 x''^2}{\xi^2}\right)\right] \tag{4.4}$$

where $A(\theta_1, \theta_2)=|E_0|^4(1+\cos\theta_1)^2(1+\cos\theta_2)^2W^5\pi^{5/2}/2\lambda^4R^4$. The factor $\exp(-x''^2/W^2)$ may be set equal to unity and x'' set equal to zero in the limits of integration to order $\xi^2/W^2\phi_0^2$ (which is small if $\phi_0 \gg 1$ and $\xi < W$). (4.4) can then be integrated to give

$$I_1 = \frac{A(\theta, \theta)W^2\xi\pi^{3/2}}{16\phi_0}\,\mathrm{erf}^2\left(\frac{\xi}{W\sqrt{2}}\right)\exp\left(-\frac{k^2\xi^2\sin^2\theta}{4\phi_0^2}\right). \tag{4.5}$$

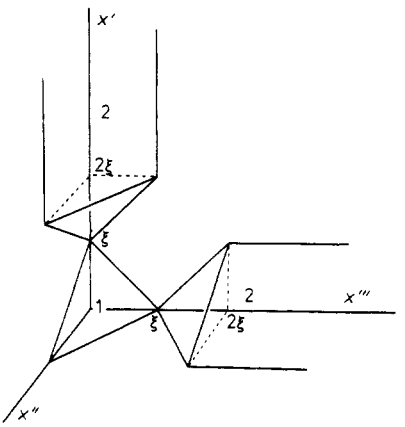

Figure 11. Regions of integration in the Fraunhofer limit.

In the region 2 of figure 11 which lies along the x' axes $G(x', x'', x''')=2(x''^2+x'''^2)/\xi^2$. The two parts of this region give equal contributions so the sum may be expressed in the form

$$I_2 = 2A(\theta, \theta)\int_0^{\xi} dx'' \int_0^{\xi-x''} dx''' \int_{\xi+x''+x'''}^{\infty} dx' \cos(2kx'' \sin\theta) \times \exp\left[-\left(\frac{x'^2+x''^2+x'''^2}{W^2}+\frac{2\phi_0^2(x''^2+x'''^2)}{\xi^2}\right)\right]. \tag{4.6}$$

To order $\xi^2/W^2\phi_0^2$ the factor $\exp[-(x''^2+x'''^2)/W^2]$ may be set equal to unity and x'' and x''' set equal to zero in the limits of integration. This leads to the result

$$I_2 = \frac{A(\theta, \theta)W\xi^2\pi^{3/2}}{8\phi_0^2}\left[1-\mathrm{erf}\left(\frac{\xi}{W}\right)\right]\exp\left(-\frac{k^2\xi^2\sin^2\theta}{2\phi_0^2}\right). \tag{4.7}$$

As in the Fresnel limit, the remaining parts of the region of integration contribute terms of order $1/\phi_0$ or less and these may be neglected if $\phi_0 \gg 1$. Thus, combining (4.5), (4.7) and (4.2) we finally obtain for the scintillation index

$$S = 1 - 2\,\mathrm{erf}\left(\frac{\xi}{W}\right) + \frac{W\phi_0}{\xi}\,\mathrm{erf}^2\left(\frac{\xi}{W\sqrt{2}}\right)\exp\left(\frac{k^2\xi^2\sin^2\theta}{4\phi_0^2}\right). \tag{4.8}$$

The spatial coherence function can be evaluated with the help of the same division of the volume of integration. Thus the contribution from region 1 of figure 11 is

$$I_1 = A(\theta_1, \theta_2)\int_0^{\xi} \mathrm{d}x'' \int_0^{\xi - x''} \mathrm{d}x''' \int_0^{\xi - x'' - x'''} \mathrm{d}x' \cos(kx''U)\cos(kx'''V) \times \exp\left[-\left(\frac{x'^2 + x''^2 + x'''^2}{W^2} + \frac{4\phi_0^2 x''^2}{\xi^2}\right)\right]. \tag{4.9}$$

We evaluate this integral under the assumption $\xi \ll W$. Setting $W^{-2} = 0$ in (4.9) and noting that $kV\xi/\phi_0 \ll 1$ over the physically interesting range of values of V for which decorrelation takes place (a point discussed further in § 5) we obtain

$$I_1 = \frac{A(\theta_1, \theta_2)\xi^3\sqrt{\pi}}{8\phi_0}\left(\frac{\sin(kV\xi/2)}{kV\xi/2}\right)^2 \exp\left(-\frac{k^2U^2\xi^2}{16\phi_0^2}\right). \tag{4.10}$$

Contributions from the two regions 2 are not equal but with a transformation of coordinates the total may be expressed in the form

$$I_2 = A(\theta_1, \theta_2)\int_0^{\xi} \mathrm{d}x'' \int_0^{\xi - x''} \mathrm{d}x''' \int_{\xi + x'' + x'''}^{\infty} \mathrm{d}x' \cos(kx''U)[\cos(kx'''V) + \cos(kx'V)] \times \exp\left[-\left(\frac{x'^2 + x''^2 + x'''^2}{W^2} + \frac{2\phi_0^2}{\xi^2}(x''^2 + x'''^2)\right)\right]. \tag{4.11}$$

This integral may be evaluated to the same order of approximation as (4.10) giving

$$I_2 = \frac{A(\theta_1, \theta_2)W\xi^2\pi^{3/2}}{16\phi_0^2}\left[1 + \exp\left(-\frac{k^2V^2W^2}{4}\right) - \frac{2\xi}{W\sqrt{\pi}}\left(1 + \frac{\sinh(kV\xi)}{kV\xi}\right)\right]\exp\left(-\frac{k^2U^2\xi^2}{16\phi_0^2}\right). \tag{4.12}$$

Neglecting the contributions from the remaining parts of the region of integration which as before are down by a factor of at least $1/\phi_0$, adding (4.10) to (4.12) and normalising the result using (4.2) leads to the coherence function ($kV\xi/\phi_0 \ll 1$)

$$g^{(2)}(\theta_1, \theta_2) = 1 + |g^{(1)}(\theta_1, \theta_2)|^2 - \frac{2\xi}{W\sqrt{\pi}}\left(1 + \frac{\sin(kV\xi)}{kV\xi}\right) + \frac{2\xi\phi_0}{\pi W}\left(\frac{\sin(kV\xi/2)}{kV\xi/2}\right)^2 \times \exp\left(\frac{k^2U^2\xi^2}{16\phi_0^2}\right). \tag{4.13}$$

Here $|g^{(1)}(\theta_1, \theta_2)|$ is defined by (4.3). Equation (4.13) reduces to $S + 1$ (equation (4.8)) when $\theta_1 = \theta_2$ provided that $\xi \ll W$; it is plotted in figure 12.

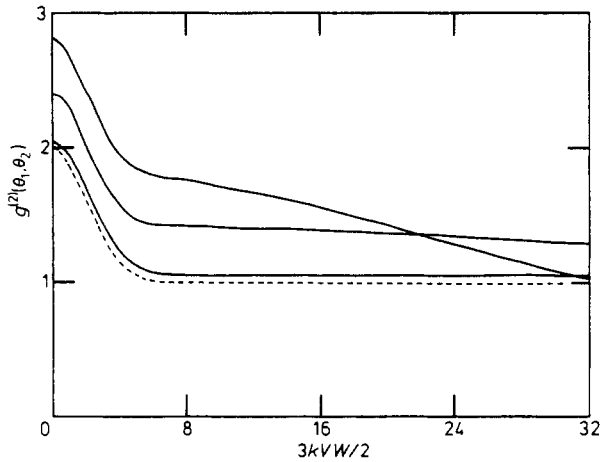

Figure 12. Spatial coherence function of intensities for the values of ξ/W shown: truncated parabolic phase autocorrelation function, Fraunhofer limit, $\phi_0^2 = 100$. The broken curve is a plot of the interference contribution obtained in the case of the truncated linear phase autocorrelation function (equation (4.22) of the text).

4.2. Truncated linear correlation function (model (b) of § 2.2)

As in case (*a*) (§ 2.2) the cut-off in $\rho(r)$ may be neglected during the evaluation of (2.23). To order $\exp(-\phi_0^2)$ we obtain

$$\langle \mathscr{E}^+(\theta_1)\mathscr{E}^-(\theta_2)\rangle = \frac{|E_0|^2(1+\cos\theta_1)(1+\cos\theta_2)W^3\xi(2\pi)^{3/2}\exp(-k^2V^2W^2/8)}{8\lambda^2R^2\phi_0^2[1+(kU\xi/2\phi_0^2)^2]}. \tag{4.14}$$

At $\theta_1 = \theta_2 = \theta$ this reduces to the angular distribution of intensity

$$\langle I(\theta)\rangle = \frac{|E_0|^2(1+\cos\theta)^2W^3\xi(2\pi)^{3/2}}{8\lambda^2R^2\phi_0^2[1+(k\xi\sin\theta/\phi_0^2)^2]}. \tag{4.15}$$

The presence of the exponential factor in (4.14) implies that $kV\xi/\phi_0^2 < \xi/W\phi_0^2 \ll 1$ in the region where the function is not vanishingly small so that $kU\xi/2\phi_0^2 \sim k\xi\sin\theta/\phi_0^2$ and to order $\xi/W\phi_0^2$ the normalised correlation function is therefore given by

$$g^{(1)}(\theta_1, \theta_2) = \exp(-k^2V^2W^2/8). \tag{4.16}$$

In order to evaluate the scintillation index we refer again to figure 11. The contribution from region 1 is symmetrically disposed about the x'–x''' plane through the x'' axis and we need only double the result from one of these regions, say $x' > x'''$. A further trisection of this volume is necessary before the integrals can be evaluated however, defined by $x'' < x'''$, $x' > x''$; $x'' > x'''$, $x' > x''$; and $x'' > x'$, $x'' > x'''$. The total contribution from region 1 may thus be expressed in the form

$$I_1 = 2A(\theta,\theta)\left\{\int_0^{\xi/3} dx'' \int_{x''}^{(\xi-x'')/2} dx''' \int_{x'''}^{\xi-x''-x'''} dx' \cos(2kx''\sin\theta)\right.$$
$$\left.\times\exp\left[-\left(\frac{x'^2+x''^2+x'''^2}{W^2}+\frac{2\phi_0^2x'''}{\xi}\right)\right]\right.$$

$$+\int_0^{\xi/3} dx''' \int_{x'''}^{(\xi-x''')/2} dx'' \int_{x''}^{\xi-x''-x'''} dx' \cos(2kx'' \sin\theta)$$
$$\times \exp\left[-\left(\frac{x'^2+x''^2+x'''^2}{W^2}+\frac{2\phi_0^2 x''}{\xi}\right)\right]$$
$$+\int_0^{\xi/3} dx''' \int_{x'''}^{(\xi-x''')/2} dx' \int_{x'}^{\xi-x'''-x'} dx'' \cos(2kx'' \sin\theta)$$
$$\times \exp\left[-\left(\frac{x'^2+x''^2+x'''^2}{W^2}+\frac{\phi_0^2}{\xi}(4x''-2x')\right)\right]\Bigg\} \tag{4.17}$$

where $A(\theta_1, \theta_2)$ is defined as in (4.4) above. We shall evaluate the integrals in the limit $\xi \ll W$, setting $W^{-1}=0$ in the exponents and discarding terms of order $\exp(-\phi_0^2)$. The contribution of the last term in (4.17) is down by a factor $1/\phi_0^2$ on the first two and when this is neglected we obtain

$$I_1 = A(\theta, \theta)\xi^3/\phi_0^4[1+(k\xi \sin\theta/\phi_0^2)^2]^2. \tag{4.18}$$

Regions 2 give equal contributions but further subdivision of the volumes is necessary before the integrals can be evaluated. For example the region lying along the x' axis must be considered in two parts according as x'' is less than or greater than x'''. The total contribution may be written

$$I_2 = 2A(\theta, \theta)\Bigg\{\int_0^{\xi/2} dx'' \int_{x''}^{\xi-x''} dx''' \int_{\xi+x''+x'''}^{\infty} dx' \cos(2kx'' \sin\theta)$$
$$\times \exp\left[-\left(\frac{x'^2+x''^2+x'''^2}{W^2}+\frac{2\phi_0^2 x'''}{\xi}\right)\right]$$
$$+\int_0^{\xi/2} dx''' \int_{x'''}^{\xi-x'''} dx'' \int_{\xi+x''+x'''}^{\infty} dx' \cos(2kx'' \sin\theta)$$
$$\times \exp\left[-\left(\frac{x'^2+x''^2+x'''^2}{W^2}+\frac{2\phi_0^2 x''}{\xi}\right)\right]\Bigg\}. \tag{4.19}$$

The integrals can be evaluated in the limit $\xi \ll W$ as before. Retaining up to first-order terms in (ξ/W) we obtain

$$I_2 = \frac{A(\theta, \theta)W\xi^2\sqrt{\pi}(1-2\xi/W\sqrt{\pi})}{2\phi_0^4[1+(k\xi \sin\theta/\phi_0^2)^2]^2}. \tag{4.20}$$

Adding (4.20) to (4.18) and normalising the result using (4.15) we note that the (ξ/W) term in (4.20) *exactly cancels* with the contribution (4.18) giving the Gaussian result

$$S = 1 \tag{4.21}$$

which may be contrasted with (4.8).

Evaluation of the spatial coherence function proceeds in an exactly analogous way and, as might be expected, leads in the same order of approximation to the Gaussian factorisation property

$$g^{(2)}(\theta_1, \theta_2) = 1 + |g^{(1)}(\theta_1, \theta_2)|^2 \tag{4.22}$$

where $|g^{(1)}(\theta_1, \theta_2)|$ is given by (4.16). For comparison this function is plotted against V in figure 12.

4.3. Gaussian phase correlation function (model (c) of § 2.2)

To order $\exp(-\phi_0^2)$ the results for the field coherence function and mean intensity are identical with those for the parabolic phase correlation function given by equations (4.1)–(4.3). The scintillation index may be evaluated by an extension of the method used in the Fresnel limit. The major contribution to the integral (2.12) comes from the region where $G(x', x'', x''')$ is a minimum. The derivatives of this function, with respect to each variable, vanish for all x' when $x'' = x''' = 0$ and for all x''' when $x'' = x' = 0$. $G(x', x'', x''')$ in fact attains its minimum in three dimensions everywhere on the x' and x''' axes. Taking advantage of the various symmetry properties of the integrand when $\theta_1 = \theta_2 = \theta$ we obtain the reduced formula

$$\langle I^2(\theta)\rangle = 2A(\theta,\theta)\int_0^\infty dx''\int_0^\infty dx'\int_0^{x'} dx''' \cos(2kx''\sin\theta) \times \exp\left[-\left(\frac{x'^2+x''^2+x'''^2}{W^2}+\phi_0^2 G(x', x'', x''')\right)\right] \tag{4.23}$$

and we evaluate this integral by expanding $G(x', x'', x''')$ about $x'' = x''' = 0$ (the major contribution coming from near the x' axis), i.e.

$$G(x', x'', x''') = G(x', 0, 0) + \frac{x'''^2}{2}\frac{\partial^2}{\partial x'''^2}G(x', x'', x''')\Big|_{x''=x'''=0} + \frac{x''^2}{2}\frac{\partial^2}{\partial x''^2}G(x', x'', x''')\Big|_{x''=x'''=0} \tag{4.24}$$

(4.23) then becomes

$$\langle I^2(\theta)\rangle = 2A(\theta,\theta)\int_0^\infty dx''\int_0^\infty dx'\int_0^{x'} dx''' \cos(2kx''\sin\theta) \times \exp\left(-\left\{\frac{x'^2+x''^2+x'''^2}{W^2}+\frac{2\phi_0^2 x''^2}{\xi^2}\left[1+\exp\left(-\frac{x'^2}{\xi^2}\right)\left(1-\frac{2x'^2}{\xi^2}\right)\right]\right.\right. + \left.\left.\frac{2\phi_0^2 x'''^2}{\xi^2}\left[1-\exp\left(-\frac{x'^2}{\xi^2}\right)\left(1-\frac{2x'^2}{\xi^2}\right)\right]\right\}\right) \tag{4.25}$$

and integrating over x'' and x''' yields, to order $\xi^2/W^2\phi_0^2$

$$\langle I^2(\theta)\rangle = \frac{A(\theta,\theta)\pi}{2}\int_0^\infty dx' \frac{\operatorname{erf}\left(x'\left\{\frac{1}{W^2}+\frac{2\phi_0^2}{\xi^2}\left[1-\exp\left(-\frac{x'^2}{\xi^2}\right)\left(1-\frac{2x'^2}{\xi^2}\right)\right]\right\}^{1/2}\right)}{\left\{\frac{1}{W^2}+\frac{2\phi_0^2}{\xi^2}\left[1-\exp\left(-\frac{x'^2}{\xi^2}\right)\left(1-\frac{2x'^2}{\xi^2}\right)\right]\right\}^{1/2}} \times \frac{\exp\left[-\left(\frac{x'^2}{W^2}+\left\{\frac{k^2\xi^2\sin^2\theta}{2\phi_0^2}\left[1+\exp\left(-\frac{x'^2}{\xi^2}\right)\left(1-\frac{2x'^2}{\xi^2}\right)\right]^{-1}\right\}\right)\right]}{\left\{\frac{2\phi_0^2}{\xi^2}\left[1+\exp\left(-\frac{x'^2}{\xi^2}\right)\left(1-\frac{2x'^2}{\xi^2}\right)\right]\right\}^{1/2}}. \tag{4.26}$$

This may be evaluated using the approximate model (3.25) employed in the Fresnel calculations of the last section. The main contribution to (4.26) in the region $x' < \xi/\sqrt{3}$ comes from near $x' = 0$ so we set x' equal to zero in the denominator of the second factor in the integrand and also in the denominator of the exponent appearing in the same factor. Taking advantage of the inequality $\phi_0 W/\xi \gg 1$, (4.26) is given approximately by the equation

$$\langle I^2(\theta)\rangle = \frac{A(\theta,\theta)\pi\xi^3}{4\phi_0^2\sqrt{6}} \int_0^{\xi/\sqrt{3}} \frac{dx'}{x'} \operatorname{erf}\left(\frac{x'^2\phi_0}{\xi^2}\sqrt{6}\right) \exp\left(-\frac{k^2\xi^2 \sin^2\theta}{4\phi_0^2}\right) \exp\left(-\frac{x'^2}{W^2}\right)$$
$$+ \frac{A(\theta,\theta)\pi\xi^2}{4\phi_0^2} \int_{\xi/\sqrt{3}}^{\infty} dx' \exp\left(-\frac{x'^2}{W^2}\right) \exp\left(-\frac{k^2\xi^2 \sin^2\theta}{2\phi_0^2}\right). \tag{4.27}$$

The first integral in (4.27) is evaluated by parts, taking advantage of the fact that $\phi_0 \gg 1$. The result, to order $\exp(-\phi_0^2)$ and ξ^2/W^2 is

$$I_1 = \frac{A(\theta,\theta)\pi\xi^3}{16\phi_0^2\sqrt{6}} \exp\left(-\frac{k^2\xi^2 \sin^2\theta}{4\phi_0^2}\right) \ln\left(\frac{8\gamma\phi_0^2}{3}\right). \tag{4.28}$$

The second integral in (4.27) is just an error function:

$$I_2 = \frac{A(\theta,\theta)\pi^{3/2}W\xi^2}{8\phi_0^2} \operatorname{erfc}\left(\frac{\xi}{W\sqrt{3}}\right) \exp\left(-\frac{k^2\xi^2 \sin^2\theta}{2\phi_0^2}\right). \tag{4.29}$$

After normalisation using equation (4.2) the final result for the scintillation index is (retaining terms of order ξ/W only)

$$S = 1 - \frac{4\xi}{W(3\pi)^{1/2}} + \frac{\xi}{W(6\pi)^{1/2}} \exp\left(\frac{k^2\xi^2 \sin^2\theta}{4\phi_0^2}\right) \ln\left(\frac{8\gamma\phi_0^2}{3}\right). \tag{4.30}$$

The corresponding spatial coherence function can also be evaluated analytically with the help of the approximate model (3.25). We first use the Taylor expansion (4.24) to reduce the general formula (2.24). After an integration over the x'' coordinate and normalisation using (4.2) we obtain

$$g^{(2)}(\theta_1,\theta_2) = \frac{8\phi_0^2}{\pi W\xi^2} \exp\left(\frac{k^2\xi^2}{8\phi_0^2}(U^2+V^2)\right) \int_0^{\infty} dx' \int_0^{x'} dx'''$$
$$\times \frac{[\cos(kVx') + \cos(kVx''')] \exp[-(x'^2+x'''^2)/W^2]}{[\![(2\phi_0^2/\xi^2)\{1+e^{-x'^2/\xi^2}[1-(2x'^2/\xi^2)]\}]\!]^{1/2}}$$
$$\times \exp\left(-\left\{\frac{k^2U^2\xi^2}{8\phi_0^2}\left[1+\exp\left(-\frac{x'^2}{\xi^2}\right)\left(1-\frac{2x'^2}{\xi^2}\right)\right]\right.\right.^{-1}$$
$$\left.\left. + \frac{2\phi_0^2x'''^2}{\xi^2}\left[1-\exp\left(-\frac{x'^2}{\xi^2}\right)\left(1-\frac{2x'^2}{\xi^2}\right)\right]\right\}\right). \tag{4.31}$$

Some numerically computed results based on this formula are shown in figure 13. Following the procedure used to evaluate (4.26), equation (4.31) can be expressed

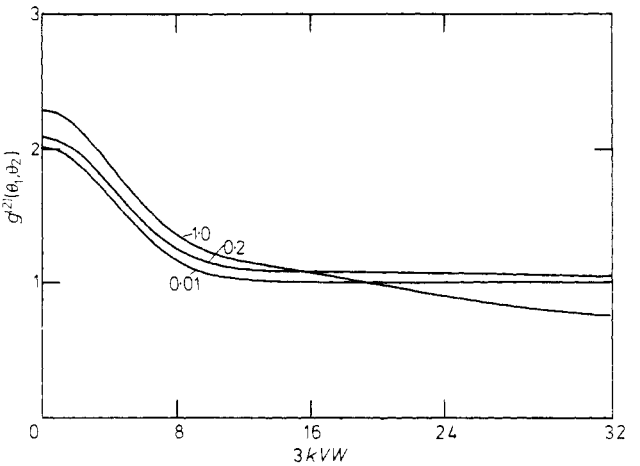

Figure 13. Spatial coherence function of intensities for the values of ξ/W shown: Gaussian phase autocorrelation function, Fraunhofer limit, $\phi_0^2 = 100$, $U = 0$.

approximately as the sum of two (double) integrals:

$$g^{(2)}(\theta_1,\theta_2) = \frac{4\phi_0}{\pi W\xi}\exp\left(\frac{k^2\xi^2}{16\phi_0^2}(U^2+2V^2)\right)\int_0^{\xi/\sqrt{3}} dx' \int_0^{x'} dx'''[\cos(kVx')+\cos(kVx''')]$$
$$\times\exp\left(-\frac{6\phi_0^2 x'''^2 x'^2}{\xi^4}\right)$$
$$+\frac{8\phi_0}{\pi W\xi\sqrt{2}}\exp\left(\frac{k^2\xi^2V^2}{8\phi_0^2}\right)\int_{\xi/\sqrt{3}}^{\infty} dx' \int_0^{x'} dx'''[\cos(kVx')+\cos(kVx''')]$$
$$\times\exp\left[-\left(\frac{2\phi_0^2 x'''^2}{\xi^2}+\frac{x'^2}{W^2}\right)\right]. \tag{4.32}$$

A little manipulation converts the first double integral into the form

$$I_1 = \frac{4\phi_0}{\pi W\xi}\exp\left(\frac{k^2\xi^2}{16\phi_0^2}(U^2+2V^2)\right)\int_0^{\xi/\sqrt{3}} dx'\cos(kVx')\int_0^{\xi/\sqrt{3}} dx'''\exp\left(-\frac{6\phi_0^2 x'''^2 x'^2}{\xi^4}\right). \tag{4.33}$$

The transformation $x''' \to x'''/x'$ followed by an integration by parts neglecting terms of order $\exp(-\phi_0^2)$ as usual, leads to the result

$$I_1 = \frac{2\xi}{W(6\pi)^{1/2}}\exp\left(\frac{k^2\xi^2}{16\phi_0^2}(U^2+2V^2)\right)\left[\mathrm{Ci}\left(\frac{kV\xi}{\sqrt{3}}\right)+\frac{1}{2}\mathrm{E}_1\left(\frac{k^2V^2\xi^2}{8\phi_0^2}\right)\right] \tag{4.34}$$

where, as before, $\mathrm{E}_1(x)$ and $\mathrm{Ci}(y)$ are the exponential and cosine integrals respectively. The second double integral in (4.32) may also be evaluated to order $\exp(-\phi_0^2)$ and the result expressed in terms of complex error functions:

$$I_2 = \mathrm{Re}\,\mathrm{erfc}\left(\frac{\xi}{W\sqrt{3}}+\frac{ikVW}{2}\right)\exp\left[\frac{k^2V^2}{4}\left(\frac{\xi^2}{2\phi_0^2}-W^2\right)\right]+\mathrm{erfc}\left(\frac{\xi}{W\sqrt{3}}\right). \tag{4.35}$$

Formulae (4.34) and (4.35) reduce to the appropriately normalised form of (4.28) and (4.29) respectively if $V = 0$. In order to facilitate interpretation of these results we

expand (4.35) in powers of ξ/W retaining only up to first-order terms in this small quantity. If we also set $U=0$ for simplicity we have, finally, from (4.34) and (4.35)

$$g^{(2)}(\theta_1, \theta_2) = 1 + |g^{(1)}(\theta_1, \theta_2)|^2 - \frac{2\xi}{W(3\pi)^{1/2}} \exp\left(\frac{k^2V^2\xi^2}{8\phi_0^2}\right)\left[\exp\left(-\frac{k^2V^2\xi^2}{8\phi_0^2}\right) + \frac{\sin(kV\xi/\sqrt{3})}{kV\xi/\sqrt{3}}\right] + \frac{2\xi}{W(6\pi)^{1/2}} \exp\left(\frac{k^2V^2\xi^2}{8\phi_0^2}\right)\left[\mathrm{Ci}\left(\frac{kV\xi}{\sqrt{3}}\right) + \frac{1}{2}\mathrm{E}_1\left(\frac{k^2V^2\xi^2}{8\phi_0^2}\right)\right] \tag{4.36}$$

where $|g^{(1)}(\theta_1, \theta_2)|$ is given by (4.3). Plots of (4.36) compare favourably with results obtained numerically from equation (4.31) when ξ/W is small.

5. Discussion

In the first part of this section we comment briefly on the general results obtained in § 2. Most of the discussion is reserved for the deep phase screen limit analysed in §§ 3 and 4, however. In the second part of the section we show how those terms in our formulae connected with the presence of speckle in the scattered intensity pattern and those connected with other scintillation effects such as focusing may be identified and distinguished. This enables the mathematical origin of the phenomena to be established and facilitates a more detailed discussion of the theoretical predictions in the last part of the section.

5.1. General results

The most widely accepted result given in § 2 appears to be equation (2.11) which implies that the field coherence function is the same at all planes in the Fresnel region (2.5). This relation was first established and discussed by Booker *et al* (1950) and we shall find later that as a consequence, in the Fresnel limit the coherence length characterising that component of the intensity pattern which arises from interference effects (i.e. the speckle) is independent of distance from the screen.

The general asymptotic formulae (2.18)–(2.22) for the intensity statistics, which hold far from the screen in the Fresnel limit, have not been given before, although Mercier (1962) derived a special case of these results assuming joint Gaussian statistics for the phase function. Our treatment of the problem, whilst not mathematically rigorous, is plausible and gives physically reasonable results. The basic premise leading to these formulae is that the real and imaginary parts of the complex amplitude far from the screen constitute a circular complex Gaussian process. This property in turn follows if : (*a*) the memory condition (2.14) is satisfied so that far from the screen the scattered field is composed of many independent contributions and the central limit theorem can be applied; and (*b*) the Fresnel condition (2.5) is satisfied so that the systematic phase factor in the vector addition of the independent contributions distributes the noise in the resultant amplitude in a uniform fashion, i.e. the variances of the real and imaginary parts of this complex amplitude are equal. We emphasise again here that unmodified power law structure functions do not satisfy (2.14) and their use in phase screen calculations could give incorrect statistical properties unless $\phi_0 \gg 1$ when, as pointed out below, the calculations may become insensitive to the tail of the phase autocorrelation function. Fried (1976) has recently suggested that the scattered intensity should be

Rice distributed even in the Fraunhofer limit (2.6). However, specific counter examples can be found to this prediction (e.g. Goodman 1975) and in general it may be asserted that in the limit (2.6) the scattered field should constitute a circular complex Gaussian process only when the phase shifts introduced by the screen are large (i.e. $\phi_0 \gg 1$) and the illuminated area contains many phase correlation lengths. The mean amplitude is then zero, the scattered intensity negative exponentially distributed and the first- and second-order coherence functions are related by the characteristic factorisation property (2.28). Optical frequency radiation with these properties is usually referred to as 'Gaussian light' and the associated intensity pattern is sometimes described as 'fully developed speckle'. In the discussion of the deep phase screen limit which follows we shall use the terms 'Gaussian statistics' or 'Gaussian limit' as abbreviated references to this situation.

5.2. Deep phase screen limit: qualitative features

Interpretation of the results presented in §§ 3 and 4 is facilitated by comparison with the simple discrete scatterer model described in our previous papers (Jakeman 1974, Jakeman and Pusey 1975, 1976, Jakeman *et al* 1976). In this model we assume that the scattered field is composed of N randomly phased contributions with amplitudes a_j which are statistically identical, independent from each other and from the phases ϕ_j:

$$\mathscr{E}^{+}(\boldsymbol{r}, t) = \sum_{j=1}^{N} a_j(\boldsymbol{r}) \exp(\mathrm{i}\phi_j(\boldsymbol{r})) \exp(\mathrm{i}\omega t). \tag{5.1}$$

The scintillation index and second-order spatial coherence function may be written

$$S + 1 = 2\left(1 - \frac{1}{N}\right) + \frac{\langle a^4 \rangle}{N\langle a^2 \rangle^2} \tag{5.2}$$

$$g^{(2)}(\boldsymbol{r}, \boldsymbol{r}') = \left(1 - \frac{1}{N}\right)(1 + |g^{(1)}(\boldsymbol{r}, \boldsymbol{r}')|^2) + \frac{\langle a^2(\boldsymbol{r}) a^2(\boldsymbol{r}') \rangle}{N\langle a^2(\boldsymbol{r}) \rangle \langle a^2(\boldsymbol{r}') \rangle} \tag{5.3}$$

where

$$|g^{(1)}(\boldsymbol{r}, \boldsymbol{r}')| = \frac{\langle a(\boldsymbol{r}) a(\boldsymbol{r}') \rangle}{(\langle a^2(\boldsymbol{r}) \rangle \langle a^2(\boldsymbol{r}') \rangle)^{1/2}} |\langle \exp[\mathrm{i}(\phi(\boldsymbol{r}) - \phi(\boldsymbol{r}'))] \rangle|. \tag{5.4}$$

The terms containing N in (5.2) and (5.3) quantify the deviation from Gaussian field statistics for this simple model when the number of scatterers is finite. In the limit $N \to \infty$ the scintillation index approaches unity and from equation (5.3) we recover the factorisation theorem characteristic of a zero-mean circular complex Gaussian process. The 'Gaussian' or interference term $|g^{(1)}(\boldsymbol{r}, \boldsymbol{r}')|^2$, associated with speckle in the scattered intensity pattern is clearly identifiable in (5.3) even when N is finite; however, its magnitude is reduced and there is in addition a 'single-scatterer' or 'non-Gaussian' term dependent on the properties of the individual scatterers. This latter term will be present even in incoherent scattering situations when intensities rather than fields are additive and when no interference effects are present. Even when speckle is present this non-Gaussian term may represent the dominant fluctuation in the intensity pattern if N is small and the cross section fluctuations of a single scatterer are sufficiently large.

We now seek the structure of equations (5.2) and (5.3) in the analytical results of §§ 3 and 4 in the hope of identifying terms associated with speckle and terms connected with other scintillation effects. Examining first the Fraunhofer results (§ 4) we see that

the spatial coherence functions for the truncated parabolic and Gaussian models (equations (4.13) and (4.36), respectively) are precisely of the form (5.3) if we set $N \sim W/\xi$ corresponding to independent scattering elements of length ξ at the screen. Thus in each formula we recognise first the speckle term $|g^{(1)}(\theta_1, \theta_2)|^2$ followed by a $1/N$ correction term (which is a little more complicated than in (5.3)) and finally a single-scatterer term. The corresponding scintillation indices (equations (4.8) and (4.30)) reduce to the form (5.2) when the error functions are expanded to first order in ξ/W. Note, however, that to the order of approximation in which these results are valid *no* deviation from Gaussian statistics is predicted for the truncated linear phase autocorrelation function model.

In the Fresnel limit the situation is complicated by the presence of focusing and other effects near the screen. However, we have seen in a previous paper (Jakeman and McWhirter 1976) that these phenomena may themselves be interpreted as 'single-scatterer' effects which arise because the effective area contributing to the scattered field is reduced near to the screen. It is evident from the Fraunhofer case that formulae in which only the first-order deviation from Gaussian statistics is retained most closely resemble (5.2) and (5.3). Since in the Fresnel region the scintillation index saturates to the Gaussian value of unity at large distances from the screen for all model phase correlation functions when $\phi_0 \gg 1$, we examine the departure from Gaussian statistics to first order in the reciprocal of this length. We see immediately that the asymptotic formula (3.37), derived for the spatial coherence function in the case of the Gaussian model phase autocorrelation functions is of the form (5.3) if we set $N \sim q^{-1}$. Indeed this formula is very similar to the result obtained in the Fraunhofer limit (equation (4.36)) and its terms can be interpreted in precisely the same way. In the case of the parabolic phase autocorrelation function the right-hand side of (3.10) must be expanded to first order in $1/z$ (but retaining all terms involving χ without approximation). The result obtained is

$$g^{(2)}(z, \chi) = 1 + |g^{(1)}(z, \chi)|^2 - \left(\frac{k\xi^2}{z\phi_0(2\pi)^{1/2}}\right)\left(1 + \frac{\sin(k\xi\chi/z)}{k\xi\chi/z}\right) + \left(\frac{k\xi^2}{\pi z\phi_0}\right)\phi_0\left(\frac{\sin(k\xi\chi/2z)}{k\xi\chi/2z}\right)^2. \tag{5.5}$$

This is almost identical with the Fraunhofer result if we replace $(k\xi^2/z\phi_0)$ with $2\xi/W$ and χ/z with V, and is clearly of the form (5.3) with $N \sim z\phi_0(2\pi)^{1/2}/k\xi^2 \sim q^{-1}$ as in the case of the Gaussian model. For both model phase autocorrelation functions this latter identification is consistent with the notion of an *effective* area of the screen contributing to the scattered field in the Fresnel limit. Thus the speckle size ξ/ϕ_0 (equations (3.2) or (3.21)) corresponds to an effective aperture $z\phi_0/k\xi$ at the screen, and if we assume that each scatterer occupies a length ξ as above then the total number of independent scatterers which can contribute to the field at a distance z from the screen will be $z\phi_0/k\xi^2 \sim q^{-1}$.

A similar expansion of the Fresnel results in the case of the truncated linear phase correlation function leads to qualitative different formulae. Thus, for large z, the spatial coherence function (3.19) is given approximately by

$$g^{(2)}(z, \chi) = 1 + |g^{(1)}(z, \chi)|^2 - \frac{k\xi^2}{\pi z\phi_0^4}\left[1 + \left(\frac{k\xi\chi}{2z\phi_0^2}\right)^2\right]^{-2}. \tag{5.6}$$

This is somewhat similar to (5.3) if we set $N \sim \pi z\phi_0^4/k\xi^2$: the speckle term in particular is present in the expected form. However, unlike (5.5) an *additive* non-Gaussian term is

not in evidence suggesting that fluctuations in the cross section of an individual scatterer perhaps give a contribution which is smaller than the correction to the Gaussian term. The corresponding scintillation index is in fact less than unity for all $\phi_0 \gg 1$ and z (figure 7). Further, the speckle size ξ/ϕ_0^2 (equation (3.11)) indicates an effective aperture at the screen of order $z\phi_0^2/k\xi$ so that to obtain the above value for N we require the independent scattering elements to be of length ξ/ϕ_0^2, i.e. equal to the coherence length of the field at the screen rather than the coherence length of the phase fluctuations. This would explain the results obtained in the Fraunhofer limit showing no deviation from Gaussian statistics since we would have $N^{-1} \sim \xi/W\phi_0^2$ in this region and such terms were specifically neglected in the calculations.

We have demonstrated above that in the Fraunhofer limit (2.6) and far from the screen in the Fresnel limit (2.5), a simple discrete scatterer model enables us to recognise interference (or speckle) terms and, at least for the truncated parabolic and Gaussian model phase autocorrelation functions, single-scatterer terms in our results. Closer examination of the analysis presented in §§ 3 and 4 and in the appendices reveals that the interference contributions including the $1/N$ correction terms always derive from regions 2 of figures 3 and 11 whilst the non-Gaussian or single-scatterer terms always originate from region 1 of these figures. This is entirely analogous to the way in which terms in the multiple summation leading to equation (5.3) separate, and allows us to identify these two types of contribution in the more complicated formulae which apply close to the screen in the Fresnel limit. This in turn facilitates the more detailed interpretation of results described below.

5.3. Deep phase screen limit; detailed interpretation of results

5.3.1. Truncated parabolic phase autocorrelation function. Inspection of the Fraunhofer results (4.8) and (4.13) shows that this function generates a one-dimensional analogue of the facet model discussed at length in previous publications (Jakeman 1974, Jakeman and Pusey 1975). The independent scatterers in this model are flat facets of equal size ξ and Gaussian slope distribution. The number of potential scatterers in the Fraunhofer limit is thus W/ξ as indicated in the earlier discussion but the single-scatterer terms in (4.8) and (4.13) are enhanced by cross section fluctuations due to the distribution of slopes present in the illuminated region. The enhancement factor is inversely proportional to the probability of finding a facet whose diffraction lobe falls on the receiver; it is therefore proportional to the RMS phase shift ϕ_0 and increases in a Gaussian fashion with angle (equation (4.8)). This may be contrasted with the angle dependence of the mean intensity (4.2) which is *directly* proportional to the probability of finding a facet facing the receiver. These effects are discussed at greater length in e.g. Jakeman and Pusey (1975). Note that the correction to the interference term in equation (4.8) can usually be neglected by comparison with the single-scatterer term if $\xi/W \leqslant 1$ and ϕ_0 is large.

The spatial coherence function (4.13) is characterised by two angular sizes ω_1 and ω_2. One is the speckle size present in the interference term $|g^{(1)}(\theta_1, \theta_2)|^2$, and this is related to the size of the illuminated region in the usual way according to equation (4.3): $\omega_1 \sim (kW)^{-1}$. The other, present in the single-particle term, is clearly related to the far field diffraction pattern of a single facet. This term decays in inverse proportion to the square of the angular separation of the receiver, V, and exhibits an oscillatory structure of angular period $\omega_2 \sim (k\xi)^{-1}$. The correction to the Gaussian term dependent on V can be neglected if $\phi_0 \gg 1$. Since (4.13) is only valid when $\xi \ll W$ we have $\omega_2 \gg \omega_1$ so that the

speckle and non-Gaussian contributions are clearly distinguishable in plots of this function (figure 12). One further point which must be mentioned here is that (4.13) was derived under the assumption $kV\xi/\phi_0 \ll 1$ because both Gaussian and non-Gaussian contributions to the spatial coherence function decorrelate (i.e. decay to zero) before $kV\xi/\phi_0$ is significant if $\phi_0 \gg 1$.

In the Fresnel limit we might expect the effective area contributing to the scattered field to be determined by the slope distribution of the facets which will limit the number of these scatterers giving 'specular' contributions to a given receiving point. The RMS tilt of a facet is of order $\phi_0/k\xi$ so that the length of the screen which can contribute at a point z will be $z\phi_0/k\xi$. This implies a speckle size ξ/ϕ_0 and number of potential scatterers $z\phi_0/k\xi^2$ confirming our interpretation of (5.5) and in agreement with equations (3.2) and (3.10). The principal peak in the scintillation index (3.6) plotted in figure 4 occurs at the diffraction maximum of a single facet, i.e. $z/k\xi^2 \sim 1$. The number of potential scatterers ($\sim\phi_0$) is large in this region but the non-Gaussian term in (3.6) containing Fresnel integrals is enhanced because only a few of the facets give a specular contribution to the scattered field, i.e. there are cross section fluctuations. As in the Fraunhofer limit the enhancement factor is proportional to ϕ_0 so that the RMS phase shift cancels from the single-scatterer term. The non-Gaussian term is thus important near the diffraction maximum plane $z \sim k\xi^2$ but its magnitude is limited by the large number of potential scatterers and, in contrast to the Fraunhofer limit, it does not increase in proportion to ϕ_0. Note that in the region $z\phi_0/k\xi^2 \sim 1$, where the number of contributing scatters is small, the scintillation index is considerably reduced. This is because although fewer facets contribute to the field in this region, the contrast in the diffraction pattern from an individual scatterer is less so that the enhancement factor due to cross section fluctuations is also reduced. Although the formula (3.6) approaches the correct limiting value as $z \to 0$ it may assume incorrect values when $k\xi^2/z\phi_0^2$ is not small since terms of this order have been neglected in the calculations (appendix 1). Portions of the scintillation curves near to the screen have been omitted from figure 4 for this reason.

As in the Fraunhofer limit, more than one characteristic length is present in the spatial coherence function, equation (3.10) in the Fresnel limit. The two principal scales are most easily discerned in the asymptotic result (5.5) where only the far field diffraction pattern of a single facet is involved in the non-Gaussian term. We have already discussed the speckle size, ξ/ϕ_0, associated with the $|g^{(1)}(z, \chi)|^2$ interference term in (3.10). The non-Gaussian or single-scatterer term involving Fresnel integrals falls off more slowly like $1/\chi^2$, as in the Fraunhofer limit, and shows a complicated periodic structure involving the length scales $z/k\xi$ and $(z/k)^{1/2}$ which feature in the Fresnel diffraction pattern of a single facet. Both interference and non-Gaussian contributions are visible in figure 5. Close to the screen, when on average less than one facet contributes to the scattered field ($z\phi_0/k\xi^2 < 1$), another length present in the error function corrections to the interference term in (3.10) must be taken into account, i.e. $z\phi_0/k\xi$. This characterises the limitation placed by geometrical optics on the length in the receiving plane over which rays can arrive from two adjacent facets and thus produce interference effects. It is much greater than the speckle size in the range of validity of our formulae, however, since their derivation is based on the assumption $k\xi^2/z\phi_0^2 \ll 1$.

5.3.2. Truncated linear phase autocorrelation function. One physical interpretation of this model might be that the scattered wavefront emerging from the screen is of the form

of a histogram with equal intervals of length ξ and Gaussian random height distribution. This is a facet model in which the facets are all oriented parallel to the incident wavefront. Leaving aside the question of the validity of the Huygens–Fresnel approximation for such a model (which is a problem in the case of all phase autocorrelation functions with non-vanishing first derivatives at the origin), we see that in the Fraunhofer limit (2.6) the non-Gaussian term and the correction to the interference term will be of comparable size since the cross section of every scatterer (facet) is identical. According to equations (4.18) and (4.20) these two terms in fact cancel identically to zero. Far from the screen, in the Fresnel limit, such that $k\xi^2/z\phi_0^4 \ll k\xi^2/z\phi_0^2 \ll 1$ we note that the integrals (3.12) and (3.13) for the non-Gaussian and interference contributions to the second intensity moment reduce to

$$I_1 = \frac{2k\xi^2}{\pi z\phi_0^2}; \qquad I_2 = 2 - \frac{2k\xi^2}{\pi z\phi_0^2}\left[1 + O\left(\frac{k\xi^2}{z\phi_0^4}\right)\right]. \tag{5.7}$$

As we have mentioned earlier the speckle size (equation (3.11)) implies an effective aperture at the screen of $z\phi_0^2/k\xi$. The terms proportional to z^{-1} in (5.7) are thus of order N^{-1} according to the facet model and are analogous to terms of order ξ/W in the Fraunhofer limit. As in the Fraunhofer region they cancel identically to zero when I_1 is added to $I_2(S = I_1 + I_2 - 1)$. According to the discrete scatterer model (5.2) such cancellation would be expected if the complex amplitude from each facet was itself Gaussian distributed so that a^2 obeyed a negative exponential distribution. Interpretation of the quantity ξ/ϕ_0^2 as the characteristic length of independent elements of the wavefront emerging from the screen would appear to be consistent with the above observations and also with the predicted 'higher-order' deviation from Gaussian statistics discussed in § 5.2. It also gives the appropriate length scale for the non-Gaussian contribution to the spatial coherence function manifest in equation (5.6) and is not inconsistent with the angular distribution of intensity (4.15) if this is interpreted as being governed by the diffraction lobe width of the individual scattering elements. However, the physical basis for the above explanation is rather obscure.

One interesting feature of the results (3.16) and (3.19) and (3.20) which are valid when $\phi_0 \gg 1$ is that they represent an *exact* solution of the scattering problem for the case of an unmodified linear law structure function, i.e. in the absence of the cut-off in equation (2.30). The two-dimensional analogue of this problem has been investigated by Marians (1975) using numerical techniques. The spatial coherence function plotted in figure 7 is indeed very similar in form to the result calculated by Marians and the two length scales present in equation (5.6) above are clearly visible. The spectrum of intensity fluctuations (figure 8) shows the same rather unrevealing structure obtained by Marians except at low frequencies where our result appears to fall off rather more smoothly with decreasing frequency. Note that the scintillation index (3.16) (figure 6) increases monotonically from zero at the screen to unity when $k\xi/z\phi_0^4 \gg 1$ (which may still be very close to the screen) and exhibits no non-Gaussian peak such as would be produced by focusing effects.

It must be emphasised that the analogy between our results and those of Marians can only be drawn when $\phi_0 \gg 1$. In weak scattering situations the effect of truncation is significant, contrary to the claims made by Rumsey (1975). Thus the scintillation index for an unmodified linear power law structure function always saturates at unity at sufficiently large distances from the screen whatever the value of ϕ_0. On the other hand, for the truncated autocorrelation function (2.30) it is not difficult to show that in the

limit of large z the contributions to the scintillation index from regions 1, 3, 4, 5 and 7 of figure 3 vanish for all ϕ_0 whilst $I_2 \to 2$ and $I_6 \to -\exp(-2\phi_0^2)$ so that

$$\lim_{z\to\infty} S = 1 - \exp(-2\phi_0^2). \tag{5.8}$$

This result is identical with that obtained for the Gaussian phase autocorrelation function model and is in agreement with the more generally valid formulae presented in § 2 (see e.g. equation (2.22)). These predict that far from the screen the scintillation index should saturate at a value lying between zero and unity depending on the strength of the scattering process, i.e. on the distribution of the phase function at the screen. Experimental evidence in support of this prediction has been obtained recently by Fujii and Asakura (1977). Only when $\phi_0 \gg 1$ is the value of unity attained as in the *unmodified* linear power law case discussed by Marians (1975) and Rumsey (1975). We have therefore verified, for one type of phase autocorrelation function, our conjecture that models not satisfying the physically reasonable memory condition (2.14) can lead to unphysical results in weak scattering situations. This increases doubt as to the wisdom of using such models in phase screen calculations and suggests that the implications of their use in theories of propagation through inhomogeneous media should also be carefully examined.

As a final comment on earlier investigations of the linear power law structure function we would like to point out that Rumsey's conclusion that 'the high frequency approximation to the intensity spectrum is the angular spectrum that would result from twice the strength of turbulence' is a direct consequence of the presence of the familiar Gaussian or speckle term $|g^{(1)}(z, \chi)|^2$ in expressions for the spatial coherence function and simply reflects the fact that interference is taking place in the scattered radiation.

Finally we note that in the deep phase screen limit results identical to (3.16), (3.19) and (3.20) will be obtained for any one-dimensional phase autocorrelation function with non-vanishing first derivative at the origin such as $\exp(-|x|/\xi)$. This is because in calculations of the Fresnel type (§ 3), for example, the principle contributions to the integrals again come from regions near the axes in figure 3 ($\phi_0 \gg 1$) where Taylor expansions of the phase correlation functions in $F(x, x')$ (equation (2.10)) may be used. In contrast to the case of the Gaussian model phase autocorrelation function however, when the first derivative of $\rho(x)$ at the origin is non-zero the leading terms in these expansions involve only one coordinate. Near the z axis for example, we have

$$F(x, x') = -2x' \left.\frac{\mathrm{d}\rho(x)}{\mathrm{d}x}\right|_{x=0} + \mathrm{O}(x'^2) \tag{5.9}$$

which immediately gives a formula identical to (3.15) for the scintillation index when we set $\xi = (-\mathrm{d}\rho(x)/\mathrm{d}x)_{x=0}^{-1}$.

5.3.3. Gaussian phase autocorrelation function. The results obtained using this function can again be interpreted in terms of a model in which the wavefront emerging from the screen is assumed to be composed of a number of independent elements of length ξ. Only those elements containing points which are specular with respect to the receiving direction give significant contributions to the detected intensity so that the effective number of scattering centres is reduced by a factor depending on the slope distribution of the emergent wavefront, as in the case of truncated parabolic phase autocorrelation function. This slope distribution is in fact the same for both models, depending only on

the second derivative of the phase autocorrelation function at the origin, and consequently statistical properties which it governs such as the mean intensity, first-order coherence function, speckle contribution to the scintillation index and its angle dependence, are also the same for both models. The intensity pattern associated with a single scattering centre is not the same for the two models, however, as comparison of the final terms in the Fraunhofer results (4.8) and (4.30) for the scintillation index readily reveals. The far field intensity pattern due to a flat facet is just a simple diffraction lobe whose width is inversely proportional to the facet size. On the other hand a smoothly varying wavefront will produce diffraction broadened caustics in the far field ($\phi_0 \gg 1$) whose detailed shape is governed by geometrical optics considerations as well as by diffraction (M V Berry, private communication). The characteristic width of such features depends on the distribution of curvature along the emergent wavefront (which is associated with the fourth derivative of the phase autocorrelation function at the origin) and, for the Gaussian model (2.31), is considerably greater than that of the diffraction lobe associated with a flat facet of length ξ when $\phi_0 \gg 1$. The cross section fluctuations of the scattering centres are, as a consequence, proportionally less. Thus, in the Fraunhofer limit, instead of the ϕ_0 factor of enhancement present in equation (4.8) for the scintillation index based on the truncated parabolic phase correlation function, we find a factor of only $\ln \phi_0$ in the corresponding result (4.30) based on the Gaussian phase autocorrelation function.

In the Fresnel limit, qualitative differences between the results obtained using the two models arise in the same way. The largest fluctuations in the cross section of a single scatterer in the Gaussian phase autocorrelation function case occur near the geometrical optics focus $z = k\xi^2/\phi_0$ as opposed to the diffraction maximum $z = k\xi^2$ which only has significance in this context if the scatterers are flat facets. Thus the scintillation index based on the Gaussian model exhibits a peak near $q = 1$ (figure 9). Moreover, since the number of scatterers $N \sim q^{-1}$ is of order unity at the peak, the full non-Gaussian enhancement factor proportional to $\ln \phi_0$ is retained. This may be contrasted with the parabolic case where the large number of scatterers in the region of the diffraction maximum serves to cancel the ϕ_0 enhancement in this factor. The height of the focusing peak in figure 9 is therefore proportional to $\ln \phi_0$ (contrast with figure 4). This result has been obtained by many authors using a variety of approximations (Salpeter 1967, Buckley 1971, Shishov 1971, Taylor and Infosino 1975). Buckley, in particular, obtained a formula for the scintillation index very similar to (3.34). His result is expressed in terms of length scales associated with the coefficients of the second and third terms of the Taylor expansion (2.32) of an arbitrary even powered phase correlation function. Inspection of our analysis reveals that the results do indeed depend on only the second and fourth derivatives of the Gaussian phase autocorrelation function. The exponent appearing in the integral on the right-hand side of equation (3.24) could be expressed more generally as $-\phi_0^2 x'^2(\rho''(x)-\rho''(0))$ for example and the modelling (3.25) would then take the form ($\rho'' \equiv d^2\rho/dx^2$, $\rho^{iv} \equiv d^4\rho/dx^4$)

$$\rho''(x)-\rho''(0) \simeq \begin{cases} x^2\rho^{iv}(0)/2 & x < L_4^2\sqrt{2}/L_2 \\ \rho''(0) & x > L_4^2\sqrt{2}/L_2 \end{cases} \tag{5.10}$$

where $L_2 = (-\rho''(0))^{-1/2}$, $L_4 = (\rho^{iv}(0))^{-1/4}$. The analysis subsequent to this step is identical to that described in § 3.3 and leads to the result

$$S = 1 - 2\,\mathrm{erf}(\bar{q}) + \frac{\bar{q}}{\pi}\exp(-\bar{q}^2)\left[\ln\left(\frac{8\gamma\phi_0^2 L_4^4}{L_2^4}\right) + \pi\,\mathrm{erfi}(\bar{q}) - R(\bar{q})\right] \tag{5.11}$$

where $\bar{q} = kL_4^2/z\phi_0\sqrt{2}$. This formula contains terms which are similar to, though not identical with contributions to S from various frequency ranges calculated by Buckley (1971). The coefficient of the term $\ln \phi_0$ in particular is identical to that found by Buckley (1971) and Shishov (1971). Equation (5.11) reduces to (3.34) if we set $\rho''(0) = -2\xi^{-2}$ and $\rho^{iv}(0) = 12\xi^{-4}$ appropriate to the Gaussian phase autocorrelation function.

We should like to point out that the curve corresponding to $\phi_0^2 = 8$ in figure 9 which we have computed from the intermediate approximation (3.24) is indistinguishable from that obtained by Whale (1973) who calculated the result directly from equation (2.9). Since formula (3.24) becomes more accurate as ϕ_0 increases the remaining curves in figure 9 can be regarded as essentially exact solutions of the problem. Comparison of the numerically computed curves with the analytical result (3.34) (plotted as broken curves in figure 9) shows that this formula is a good approximation for large values of ϕ_0 as expected. The largest error occurs at the peak and decreases from a little more than 15% at $\phi_0^2 = 8$ to less than 4% when $\phi_0^2 = 10^4$.

Plots of the spatial coherence function of the intensity for the Gaussian phase autocorrelation function model do not seem to have been given previously although a number of authors (e.g. Bramley and Young 1967, Buckley 1971) have quoted values for the half-width or characteristic length to the 1/e point. It is clear from figures 10 and 13 that this is not particularly useful information because several length scales are involved in the decay of this quantity. These can be identified most easily in the analytical behaviour far from the screen in the Fresnel limit (equation (3.37)). The smallest scale present in this result is the speckle size ξ/ϕ_0 associated as usual with the $|g^{(1)}(z, \chi)|^2$ interference term. Unlike the parabolic case *two* further characteristic lengths are in evidence. The origin of these can be understood from the structure of the non-Gaussian final term (containing Ci and E_1) which is larger than the correction to the interference term when $\phi_0 \gg 1$. The argument of the exponential integral is independent of wavelength if we set $\phi_0 \sim kh_0$ for a surface scattering configuration in which h_0 is the RMS surface height fluctuation. We may therefore associate this term with the distribution of intensity near a caustic predicted by geometrical optics. The corresponding length scale of the order of $z\phi_0/k\xi$ is the longest one present in equation (3.37). On the other hand, the cosine integral is clearly a diffraction term and presumably, describes the diffraction broadening of the otherwise singular behaviour of the intensity at a caustic. This term decays inversely as its argument and in an oscillatory fashion with period of the order of $z/k\xi$. This period is down by a factor ϕ_0 on the length scale associated with the geometrical optics term (E_1) and, being of order $\xi/q\phi_0$ it is greater than the speckle size when z lies beyond the focusing region.

The speckle and single-scatterer contributions are clearly visible in figure 10, but the two longer characteristic lengths cannot easily be distinguished over the range of detector separations for which the graphs are plotted. The analytical result (3.37) is in good agreement with the numerically computed curves even for values of q relatively close to the peak in the scintillation curve. According to the more exact result presented in the appendix (equations (A.37) and (A.38)) no drastic change in the behaviour of the spatial coherence function is to be expected in this region but the magnitude of the interference contribution to the statistics begins to decrease markedly. In fact the speckle size ξ/ϕ_0 and the period of the cosine integral in (3.37) are comparable in the focusing region so that the contributions of interference and diffraction cannot be easily distinguished. The characteristic length associated with the geometrical optics term, on the other hand, is still much larger, being of order ξ. Note that the dip below unity

exhibited by several of the curves in figure 10 reflects the fact that for certain receiver separations close to the screen only one scattering centre may be in the field of view of both receivers. If the 'spike' of radiation from this scatterer falls on one receiver then it cannot fall on the other so that the intensity cross-correlation coefficient will be small. As the separation of the receivers is increased further, there will come a point when each will 'see' a different independent scattering centre giving a cross-correlation coefficient of unity in agreement with the asymptotic behaviour for large χ predicted by the analytical results (3.37), (A.38) and (A.39) and with the numerically computed curves.

The form of the spatial coherence function (4.36) in the Fraunhofer limit is completely analogous to the Fresnel result (3.37) valid far from the screen and does not warrant further discussion. Thus as a final comment we merely note that all the formulae obtained in the case of the Gaussian phase autocorrelation function may be generalised along the lines indicated prior to equation (5.11) above provided the length scales L_4 and L_2 are not too dissimilar (for a discussion of this last point see Buckley 1971).

6. Summary and conclusions

We have evaluated the first- and second-order statistical properties of the intensity of radiation scattered by a deep Gaussian random phase screen for three types of phase autocorrelation function and have identified, with the help of a discrete scatterer model, those terms in our formulae which arise due to interference and are associated with speckle in the intensity pattern, and those terms which arise from single-scatterer affects and are associated with non-Gaussian variations in intensity. We have shown that a simple physical interpretation of the scattering process is possible when the phase autocorrelation function is of truncated parabolic or Gaussian form.

In the first (truncated parabolic) case the wavefront emerging from the screen can be thought of as being composed of equal sized facets with Gaussian slope distribution. In the Fresnel limit the scintillation index has a peak near the diffraction maximum of a single facet. The maximum height of this peak is independent of wavelength being limited by the fact that a large number of elementary scatterers actually contribute to the intensity in its neighbourhood. When the number of scatterers is restricted by the width of the illuminating beam as in the Fraunhofer region, however, large deviations from Gaussian statistics arise because of the sharpness of the spikes of intensity received from individual facets. These non-Gaussian fluctuations increase as the spikes sharpen up with a decrease in wavelength. In addition to the speckle size, the spatial coherence function is characterised by the width of the diffraction lobe from a single facet.

In the second (Gaussian) case the wavefront emerging from the screen can also be decomposed into a number of independent scattering elements which contribute to the detected intensity only if they contain specular points with respect to the receiving direction. In the Fresnel region these produce a peak in the scintillation index near the geometrical optics focusing plane of the wavefront. On average, only one scatterer contributes to the intensity in this region so that deviation from Gaussian statistics is larger than in the parabolic case and increases when the pattern associated with an individual scatterer is sharpened by a decrease of wavelength.

A similar wavelength dependence of non-Gaussian fluctuations is found in the Fraunhofer limit. For a given number of scatterers the size of the deviation in this limit

is considerably smaller than in the case of the truncated parabolic phase autocorrelation function, however, because the far field intensity pattern associated with a single scatterer is not a simple sharp diffraction lobe but a diffraction broadened caustic with a long 'geometrical optics' tail. In addition to the speckle size, the spatial coherence function is characterised both by a length associated with this tail and a length associated with diffraction broadening.

The analytical formulae we have derived for these two model phase autocorrelation functions (i.e. truncated parabolic and Gaussian) are supported by a large number of numerically computed results. Our original contributions here include plots of the scintillation index for very large mean square phase shifts, and plots of the associated spatial coherence functions of the intensity. Although our models are one dimensional the shape of the latter functions should not be qualitatively different in the two-dimensional case and one conclusion that cannot be avoided here is that a coherence length defined by decay to the $1/e$ point on these curves, as quoted by previous authors (e.g. Bramley and Young 1967, Buckley 1971), is not a useful characteristic because of the multiple length scales present.

Although interference terms can be identified in our results for the truncated linear phase autocorrelation function, it is difficult to formulate a simple physical picture of the scattering process which satisfactorily explains the form of deviations from Gaussian statistics in this case. No peak is predicted in the scintillation index for this model and non-Gaussian fluctuations in both Fresnel and Fraunhofer limits seem to be higher-order effects than those predicted using the other two models. One problem with this phase autocorrelation function is the implied discontinuities in the scattered wavefront associated with the non-vanishing first derivative at the origin. As we have emphasised throughout the calculations, the results obtained in the deep phase screen limit depend crucially on the behaviour of the phase autocorrelation function near the origin, so that the use of models with an unphysical behaviour in this region such as those involving odd or fractional power law dependencies must be suspect. It is true that discontinuities in the *slope* of the scattered wavefront are implicit in calculations using the truncated parabolic correlation function and associated facet model, but the simple physical interpretation of our results which is possible in this case is re-assuring and suggests that this model may be useful in scattering from some types of rigid rough surfaces (e.g. geological and man-made structures, crystallites etc). The Gaussian or more general even-powered phase correlation function (equation (2.32)) would seem to be more appropriate in the case of strong scattering by continuous media, however.

Finally, we have shown in this paper that unphysical statistical properties may be predicted by calculations involving phase autocorrelation functions which do not 'forget' or decay to zero with increasing spatial separations. We have demonstrated this point explicitly by showing that the truncated linear correlation function—which satisfies this criterion—gives results which differ significantly from those obtained using an unmodified form (i.e. with no cut-off) in the case of small RMS phase shifts. Thus one is led to doubt the wisdom of using unmodified odd or fractional power law structure functions (which are unphysical at the origin and at large spatial separations) in both very strong and very weak phase screen scattering configurations.

Acknowledgments

We are deeply indebted to Dr M V Berry of Bristol University for many stimulating and

constructive discussions during the course of this work and we would also like to thank our colleague Dr P N Pusey for his continuing help and experimental support.

Appendix 1

In this appendix we establish the order of magnitude of the approximations used in § 3.1. First we examine the integral (3.4) which may be written

$$I_2 = 2 - \frac{2}{\pi}\int_0^\infty \frac{dx'}{x'}\sin\left(\frac{k\xi}{z}x'\right)\exp\left(-\frac{2\phi_0^2 x'^2}{\xi^2}\right) + \frac{2}{\pi}\int_\xi^\infty \frac{dx'}{x'}\sin\left(\frac{k\xi}{z}x'\right)\exp\left(-\frac{2\phi_0^2 x'^2}{\xi^2}\right)$$
$$-\frac{2k}{\pi z}\int_0^\xi dx' \int_\xi^{x'+\xi} dx\, \cos\left(\frac{k}{z}xx'\right)\exp\left(-\frac{2\phi_0^2 x'^2}{\xi^2}\right). \tag{A.1}$$

We have

$$\left|\frac{2}{\pi}\int_\xi^\infty \frac{dx'}{x'}\sin\left(\frac{k\xi x'}{z}\right)\exp\left(-\frac{2\phi_0^2 x'^2}{\xi^2}\right)\right| \leqslant \frac{2}{\pi}\int_\xi^\infty \frac{dx'}{x'}\exp\left(-\frac{2\phi_0^2 x'^2}{\xi^2}\right) = \frac{E_1(2\phi_0^2)}{\pi} \tag{A.2}$$

and also

$$\left|\frac{2k}{\pi z}\int_0^\xi dx' \int_\xi^{x'+\xi} dx\, \cos\left(\frac{k}{z}xx'\right)\exp\left(-\frac{2\phi_0^2 x'^2}{\xi^2}\right)\right|$$
$$\leqslant \frac{2k}{\pi z}\int_0^\xi dx' \int_\xi^{x'+\xi} dx\, \exp\left(-\frac{2\phi_0^2 x'^2}{\xi^2}\right) = \frac{k\xi^2}{2\pi\phi_0^2 z}[1-\exp(-2\phi_0^2)]. \tag{A.3}$$

For large values of ϕ_0 (A.2) is of order $\exp(-2\phi_0^2)/\phi_0^2$ and is negligible whilst (A.3) is small except in a small region close to the screen. We shall not consider this region in the case of the parabolic correlation function since it does not contain features of physical interest in the present context. Provided that $\phi_0 \gg 1$ and $k\xi^2/z\phi_0^2 \ll 1$, (A.1) may therefore be written

$$I_2 = 2 - 2\,\mathrm{erf}\left(\frac{k\xi^2}{2z\phi_0\sqrt{2}}\right) + O\left(\frac{\exp(-2\phi_0^2)}{\phi_0^2}\right) + O\left(\frac{k\xi^2}{2\pi\phi_0^2 z}\right). \tag{A.4}$$

We now consider the contributions to the scintillation index of regions 3–7 of figure 3 in order. In region 3 $x+x' > \xi$, $|x-x'| < \xi$, $x < \xi$, $x' < \xi$ so that the contribution from this region is

$$I_3 = \frac{2k}{\pi z}\int_0^\xi dx \int_{\xi-x}^\xi dx'\, \cos\left(\frac{k}{z}xx'\right)\exp\left[\phi_0^2\left(1-\frac{(x+x')^2}{\xi^2}\right)\right]. \tag{A.5}$$

The transformation $x \to -x+\xi$, $x' \to -x'+\xi$ converts the region of integration into the area 1 of figure 3. The simple rotation $a = x+x'$, $b = x-x'$ then transforms (A.5) into the form

$$I_3 = \frac{k}{\pi z}\int_0^\xi da \int_{-a}^{+a} db\, \cos\left[\frac{k}{z}\left(\frac{a+b}{2}-\xi\right)\left(\frac{a-b}{2}-\xi\right)\right]\exp\left[\phi_0^2\left(1-\frac{(a-2\xi)^2}{\xi^2}\right)\right]. \tag{A.6}$$

The integral over b can be performed exactly to give

$$I_3 = 2\left(\frac{2k}{\pi z}\right)^{1/2} \int_0^{\xi} da\left[\cos\left(\frac{k}{4z}(a-2\xi)^2\right) C\left(a\left(\frac{k}{2\pi z}\right)^{1/2}\right) + \sin\left(\frac{k}{4z}(a-2\xi)^2\right) S\left(a\left(\frac{k}{2\pi z}\right)^{1/2}\right)\right] \exp\left[\phi_0^2\left(1-\frac{(a-2\xi)^2}{\xi^2}\right)\right] \tag{A.7}$$

and the transformation $a \to -a + \xi$ leads to

$$I_3 = 2\left(\frac{2k}{\pi z}\right)^{1/2} \int_0^{\xi} da\left[\cos\left(\frac{k}{4z}(a+\xi)^2\right) C\left((\xi-a)\left(\frac{k}{2\pi z}\right)^{1/2}\right) + \sin\left(\frac{k}{4z}(a+\xi)^2\right) S\left((\xi-a)\left(\frac{k}{2\pi z}\right)^{1/2}\right)\right] \exp\left(-\frac{\phi_0^2}{\xi^2} a(a+2\xi)\right). \tag{A.8}$$

Clearly

$$|I_3| \leqslant 2\left(\frac{2k\xi^2}{z\phi_0^2}\right)^{1/2} [\operatorname{erfc}(\phi_0) - \operatorname{erfc}(2\phi_0)] \exp(\phi_0^2) \sim \left(\frac{2k\xi^2}{\pi z\phi_0^2}\right)^{1/2} \frac{1}{\phi_0} \qquad \text{if } \phi_0 \gg 1 \tag{A.9}$$

so that the contribution from region 3 of figure 3 may be neglected except in a small region very close to the screen which has already been excluded from our calculations.

The contributions from regions 4 of figure 3 are equal and we consider only the shaded area below $x = x'$ where $x > \xi$, $x' < \xi$, $|x - x'| < \xi$, $x + x' > \xi$ so that

$$I_4 = \frac{2k}{\pi z} \int_{\xi}^{2\xi} dx \int_{x-\xi}^{\xi} dx' \cos\left(\frac{k}{z} xx'\right) \exp\left[-\phi_0^2\left(1 + \frac{x'^2 - x^2 + 2xx'}{\xi^2}\right)\right]. \tag{A.10}$$

It is difficult to proceed with this integral without approximation so we merely note that

$$\begin{aligned} |I_4| &\leqslant \frac{2k}{\pi z} \int_{\xi}^{2\xi} dx \int_{x-\xi}^{\xi} dx' \exp\left[-\phi_0^2\left(1 + \frac{x'^2 - x^2 + 2xx'}{\xi^2}\right)\right] \\ &= \frac{k\xi}{z\phi_0\sqrt{\pi}} \int_{\xi}^{2\xi} dx \exp\left[-\phi_0^2\left(1 - \frac{2x^2}{\xi^2}\right)\right]\left[\operatorname{erfc}\left(\frac{\phi_0}{\xi}(2x-\xi)\right) - \operatorname{erfc}\left(\frac{\phi_0}{\xi}(x+\xi)\right)\right] \\ &= \frac{k\xi^2}{\pi z\phi_0^2}\left[\int_{\xi}^{2\xi} dx\left(\frac{\exp[-2\phi_0^2(x-\xi)^2/\xi^2]}{2x-\xi} - \frac{\exp[-\phi_0^2(2\xi^2+2x\xi-x^2)/\xi^2]}{x+\xi}\right) + O\left(\frac{1}{\phi_0^2}\right)\right]. \end{aligned} \tag{A.11}$$

It is not difficult to show that the second integral in this expression is of order $\exp(-2\phi_0^2)$. The first term is highly peaked about $x = \xi$ if $\phi \gg 1$ and integration gives

$$|I_4| < \frac{k\xi^2}{2\sqrt{(2\pi)}z\phi_0^3}\left[1 + O\left(\frac{1}{\phi_0^2}\right)\right] + O(\exp(-2\phi_0^2)) \tag{A.12}$$

so that this contribution is also negligible except in the small region close to the screen which we have excluded from our calculations.

The contribution from region 5 of figure 3 is obtained by observing that in this region $x>\xi$, $x'>\xi$, $x+x'>\xi$, $|x-x'|<\xi$:

$$I_5=\frac{2k}{\pi z}\int_{\xi}^{2\xi}\mathrm{d}x\int_{\xi}^{3\xi-x}\mathrm{d}x'\cos\left(\frac{k}{z}xx'\right)\exp\left[-\phi_0^2\left(3-\frac{(x-x')^2}{\xi^2}\right)\right]. \tag{A.13}$$

Since $|x-x'|<\xi$ over the region of integration the exponential factor is everywhere less than $\exp(-2\phi_0^2)$ and I_5 may therefore be neglected when $\phi_0\gg 1$.

In region 6 of figure 3, $x>\xi$, $x'>\xi$, $|x-x'|>\xi$ and $x+x'>\xi$ so that

$$\begin{aligned}I_6&=\frac{2k}{\pi z}\exp(-2\phi_0^2)\int_{\xi}^{\infty}\mathrm{d}x'\int_{x'+\xi}^{\infty}\mathrm{d}x\cos\left(\frac{kxx'}{z}\right)\\&=-\frac{2}{\pi}\exp(-2\phi_0^2)\int_{\xi}^{\infty}\frac{\mathrm{d}x'}{x'}\sin\left(\frac{kx'}{z}(x'+\xi)\right).\end{aligned} \tag{A.14}$$

This integral may also be written

$$I_6=\frac{2k}{\pi z}\exp(-2\phi_0^2)\int_{2\xi}^{\infty}\mathrm{d}x'\int_{\xi}^{x'-\xi}\mathrm{d}x\cos\left(\frac{kxx'}{z}\right). \tag{A.15}$$

Adding (A.14) and (A.15) yields, with a little manipulation

$$\begin{aligned}I_6=\frac{k}{\pi z}\exp(-2\phi_0^2)\Bigg[&-\frac{z\pi}{2k}-\frac{2z}{k}\int_0^{\infty}\frac{\mathrm{d}x'}{x'}\cos\left(\frac{kx'^2}{z}\right)\sin\left(\frac{k\xi x'}{z}\right)\\&+\int_0^{\xi}\mathrm{d}x'\int_0^{x'+\xi}\mathrm{d}x\cos\left(\frac{kxx'}{z}\right)-\int_0^{2\xi}\mathrm{d}x'\int_{\xi}^{x'-\xi}\cos\left(\frac{kxx'}{z}\right)\Bigg].\end{aligned} \tag{A.16}$$

The first integral in (A.16) is

$$\frac{z\pi}{2k}\left[C\left(\left(\frac{k\xi^2}{2\pi z}\right)^{1/2}\right)+S\left(\left(\frac{k\xi^2}{2\pi z}\right)^{1/2}\right)\right].$$

The last two integrals are always less than the area of integration involved (ξ^2). Thus I_6 is of order $(k\xi^2/z)\exp(-2\phi_0^2)$ at most and may be neglected when $\phi_0\gg 1$ except in a region close to the screen of no physical interest.

Finally, in region 7 of figure 3 we have $x>\xi$, $x'>\xi$, $x+x'>\xi$, $|x-x'|<\xi$, so that, transforming to sum and difference coordinates

$$\begin{aligned}I_7=\frac{2k}{\pi z}\int_{-\xi}^{+\xi}\mathrm{d}a\int_{3\xi}^{\infty}\mathrm{d}b\exp(-3\phi_0^2)\exp\left(-\frac{\phi_0^2a^2}{\xi^2}\right)\cos\left(\frac{k}{4z}(a^2-b^2)\right)\\=\frac{4\exp(-3\phi_0^2)}{[1+(4z\phi_0^2/k\xi^2)^2]^{1/2}}\Bigg(\left\{\left[1+\left(\frac{4z\phi_0^2}{k\xi^2}\right)^2\right]^{1/2}+\frac{4z\phi_0^2}{k\xi^2}\right\}^{1/2}\\\times\left[\frac{1}{2}-C\left(3\left(\frac{k\xi^2}{2\pi z}\right)^{1/2}\right)\right]+\left\{\left[1+\left(\frac{4z\phi_0^2}{k\xi^2}\right)^2\right]^{1/2}-\frac{4z\phi_0^2}{k\xi^2}\right\}^{1/2}\\\times\left[\frac{1}{2}-S\left(3\left(\frac{k\xi^2}{2\pi z}\right)^{1/2}\right)\right]\Bigg)+\mathrm{O}(\exp(-4\phi_0^2))\\<\exp(-3\phi_0^2)\end{aligned} \tag{A.17}$$

which is negligible if $\phi_0\gg 1$.

Appendix 2

In this appendix we establish the order of magnitude of the approximation used in § 3.2. We first show that the upper limit of the first integral in (3.12) and (3.13) may be extended to infinity if $\phi_0 \gg 1$. In the case of equation (3.12) the additional contribution introduced by this approximation is

$$C = \frac{4k}{\pi z}\int_{\xi/2}^{\infty} \mathrm{d}x' \int_{x'}^{\xi - x'} \mathrm{d}x \cos\left(\frac{kxx'}{z}\right) \exp\left(-\frac{2\phi_0^2 x'}{\zeta}\right). \tag{A.18}$$

Clearly

$$|C| \leqslant \frac{8}{\pi}\int_{\xi/2}^{\infty} \frac{\mathrm{d}x'}{x'} \exp\left(-\frac{2\phi_0^2 x'}{\xi}\right) = \frac{4}{\pi} \mathrm{E}_1(+\phi_0^2). \tag{A.19}$$

This correction is of order $\exp(-\phi_0^2)/\phi_0^2$ if $\phi_0 \gg 1$ and is therefore negligible. A similar argument can be used in the case of I_2 (equation (3.13)). In order to assess the magnitude of the second integral in (3.14) we express this quantity in terms of complex Fresnel integrals:

$$\frac{8}{\pi}\int_0^{\infty} \frac{\mathrm{d}x'}{x'} \cos\left(\frac{k\xi x'}{z}\right) \sin\left(\frac{kx'^2}{z}\right) \exp\left(-\frac{2\phi_0^2 x'}{\xi}\right)$$

$$= 4\,\mathrm{Re}\left\{\left[\frac{1}{2} - C\left(l\left(1 + \frac{\mathrm{i}\phi_0^2}{\pi l^2}\right)\right)\right]^2 + \left[\frac{1}{2} - S\left(l\left(1 + \frac{\mathrm{i}\phi_0^2}{\pi l^2}\right)\right)\right]^2\right\} \tag{A.20}$$

where $l = (2z\phi_0^4/\pi k\xi^2)^{1/2}$. The maximum value of the right-hand side is achieved when the magnitude of the argument of the Fresnel integrals is a minimum. This occurs when $l \sim \phi_0$, but the argument is still large if $\phi_0 \gg 1$ and since $\frac{1}{2} - C(x) \sim x^{-1}$ and $\frac{1}{2} - S(x) \sim x^{-2}$ if x is large we see that the integral is of order $1/\phi_0^2$ at most and can therefore be neglected.

Turning now to the remaining regions of integration in figure 3 we see that the contribution of region 3 to the scintillation index is given by

$$I_3 = \frac{4k}{\pi z}\int_{\xi/2}^{\xi} \mathrm{d}x \int_{\xi - x}^{x} \mathrm{d}x' \cos\left(\frac{kxx'}{z}\right) \exp\left[-\phi_0^2\left(\frac{x}{\xi} + \frac{3x'}{\xi} - 1\right)\right]$$

$$= \frac{4k}{\pi z}\int_{\xi/2}^{\xi} \mathrm{d}x \frac{\exp[\phi_0^2(1 - 4x/\xi)]}{(kx/z)^2 + (3\phi_0^2/\xi)^2}\left[\frac{kx}{z}\sin\left(\frac{kx^2}{z}\right) - \frac{3\phi_0^2}{\xi}\cos\left(\frac{kx^2}{z}\right)\right]$$

$$- \frac{4k}{\pi z}\int_{\xi/2}^{\xi} \mathrm{d}x \frac{\exp[2\phi_0^2(x/\xi - 1)]}{(kx/z)^2 + (3\phi_0^2/\xi)^2}\left[\frac{kx}{z}\sin\left(\frac{kx(\xi - x)}{z}\right)\right.$$

$$\left. - \frac{3\phi_0^2}{\xi}\cos\left(\frac{kx(\xi - x)}{z}\right)\right]. \tag{A.21}$$

But

$$\left|\frac{4k}{\pi z}\int_{\xi/2}^{\xi} \mathrm{d}x \frac{\exp[\phi_0^2(1 - 4x/\xi)]}{(kx/z)^2 + (3\phi_0^2/\xi)^2}\left[\frac{kx}{z}\sin\left(\frac{kx^2}{z}\right) - \frac{3\phi_0^2}{\xi}\cos\left(\frac{kx^2}{z}\right)\right]\right|$$

$$\leqslant \frac{4}{\pi}\int_{\xi/2}^{\xi} \mathrm{d}x \frac{\exp[\phi_0^2(1 - 4x/\xi)]}{x}$$

$$= \frac{4}{\pi}[\exp(\phi_0^2)][\mathrm{E}_1(2\phi_0^2) - \mathrm{E}_1(4\phi_0^2)]. \tag{A.22}$$

If $\phi_0 \gg 1$ this term is of order $\exp(-\phi_0^2)/\phi_0^2$ and may be neglected. The second term may be treated similarly:

$$\left|\frac{4k}{\xi z}\int_{\xi/2}^{\xi} dx \frac{\exp[2\phi_0^2(x/\xi-1)]}{(kx/z)^2+(3\phi_0^2/\xi)^2}\left[\frac{kx}{z}\sin\left(\frac{kx(\xi-x)}{z}\right)-\frac{3\phi_0}{\xi}\cos\left(\frac{kx(\xi-z)}{z}\right)\right]\right|$$

$$<\frac{4}{\pi}\int_{\xi/2}^{\xi} dx \frac{\exp[2\phi_0^2(x/\xi-1)]}{x}$$

$$=\frac{4}{\pi}\exp(-2\phi_0^2)[\mathrm{Ei}(2\phi_0^2)-\mathrm{Ei}(\phi_0^2)]. \tag{A.23}$$

If $\phi_0 \gg 1$ this term is of order $1/\phi_0^2$ at most so that overall, I_3 is of this order at most and may be neglected.

The contribution of regions 4 of figure 3 is given by

$$I_4=\frac{4k}{\pi z}\int_0^{\xi} dx' \int_{\xi}^{x'+\xi} dx \cos\left(\frac{kxx'}{z}\right)\exp\left[-\phi_0^2\left(1+\frac{3x'}{\xi}-\frac{x}{\xi}\right)\right]. \tag{A.24}$$

Using exactly the same approach as in the case of I_3, (A.24) can be shown to be of order $1/\phi_0^2$ at most so that the contribution of I_4 to the scintillation index may be neglected to this order of accuracy.

The contribution of region 5 of figure 3 is given by

$$I_5=\frac{4k}{\pi z}\int_{\xi}^{2\xi} dx \int_{\xi}^{3\xi-x} dx' \cos\left(\frac{kxx'}{z}\right)\exp\left[-\phi_0^2\left(3-\frac{x}{\xi}+\frac{x'}{\xi}\right)\right]$$

$$=\frac{4k}{\pi z}\int_{\xi}^{2\xi} dx \frac{\exp[2\phi_0^2(x/\xi-3)]}{(kx/z)^2+(\phi_0^2/\xi)^2}\left[\frac{kx}{z}\sin\left(\frac{kx(3\xi-x)}{z}\right)-\frac{\phi_0^2}{\xi}\cos\left(\frac{kx(3\xi-x)}{z}\right)\right]$$

$$-\frac{4k}{\pi z}\int_{\xi}^{2\xi} dx \frac{\exp[\phi_0^2(x/\xi-4)]}{(kx/z)^2+(\phi_0^2/\xi)^2}\left[\frac{kx}{z}\sin\left(\frac{k\xi x}{z}\right)-\frac{\phi_0^2}{\xi}\cos\left(\frac{k\xi x}{z}\right)\right]. \tag{A.25a}$$

Using the same method as before these integrals can be shown to be of order $\exp(-2\phi_0^2)/\phi_0^2$ at most and are therefore negligible if $\phi_0 \gg 1$.

Region 6 of figure 3 gives a contribution identical to the truncated parabolic case, i.e. (A.15), which we have already shown to be negligible except in a region 'unphysically' close to the screen.

Finally the contribution from region 7 of figure 3 to the scintillation index is, after transformation to sum and difference coordinates,

$$I_7=\frac{4k}{\pi z}\int_{3\xi}^{\infty} da \int_0^{+\xi} db \cos\left(\frac{k(a^2-b^2)}{4z}\right)\exp\left[\phi_0^2\left(\frac{b}{\xi}-3\right)\right]$$

$$=\frac{8}{\pi}\left(\frac{k}{z}\right)^{1/2}\int_{\frac{3}{2}\xi\sqrt{(k/z)}}^{\infty} da \cos(a^2)\int_0^{\xi}\cos\left(\frac{kb^2}{4z}\right)\exp\left[\phi_0^2\left(\frac{b}{\xi}-3\right)\right] db$$

$$+\frac{8}{\pi}\left(\frac{k}{z}\right)^{1/2}\int_{\frac{3}{2}\xi\sqrt{(k/z)}}^{\infty} da \sin(a^2)\int_0^{\xi}\sin\left(\frac{kb^2}{4z}\right)\exp\left[\phi_0^2\left(\frac{b}{\xi}-3\right)\right] db. \tag{A.25b}$$

The first integral of each pair in this expression is a Fresnel integral whose value is always less than unity. The modulus of the second integral of each pair is always less

than $(\xi/\phi_0^2)\exp(-2\phi_0^2)$. Thus I_7 is at most of order $(k\xi^2/z\phi_0^4)^{1/2}\exp(-2\phi_0^2)$ and may be neglected if $\phi_0 \gg 1$ except in a region very close to the screen which is of no physical interest.

Appendix 3

In this appendix we evaluate an integral in § 3.3 and derive an expression for the spatial coherence function of the intensity for the Gaussian phase autocorrelation function case.

We first note that the derivation of (3.27) and (3.33) in the text involves neglecting terms of order $\exp(-2\phi_0^2)$. This can easily be demonstrated using methods similar to those described in appendices 1 and 2. Evaluation of (3.27) is most easily accomplished as follows. We first make the transformation $x \to x\xi^2/2\phi_0\sqrt{6}$, and write $q = k\xi^2/2z\phi_0\sqrt{6}$ as in the text (equation (3.32)). The integral then takes the form

$$I_1 = -\frac{2}{\pi} q \int_0^\infty \mathrm{d}x \, \ln(3x/2\phi_0\sqrt{6}) \cos(qx) \exp(-x^2/4). \tag{A.26}$$

If we set $I = I_1\pi/2q$ then

$$\mathrm{d}I/\mathrm{d}q = \int_0^\infty x \, \mathrm{d}x \, \ln(3x/2\phi_0\sqrt{6}) \sin(qx) \exp(-x^2/4) = -2qI + \pi \operatorname{erf}(q). \tag{A.27}$$

The last result is obtained through an integration by parts. This differential equation can be solved with the help of the integrating factor $\exp(q^2)$:

$$I(q) = \pi \exp(-q^2) \int_0^q \mathrm{d}x \, \exp(x^2) \operatorname{erf}(x) + I(0) \exp(-q^2). \tag{A.28}$$

$I(0)$ is a standard integral (Erdélyi 1954):

$$\begin{aligned} I(0) &= -\int_0^\infty \mathrm{d}x [\ln(x) - \ln(2\phi_0\sqrt{(6)}/3)] \exp(-x^2/4) \\ &= \frac{\sqrt{\pi}}{2} \ln \gamma + \sqrt{\pi} \ln\left(\frac{2\phi_0\sqrt{6}}{3}\right) = \frac{\sqrt{\pi}}{2} \ln\left(\frac{8\gamma\phi_0^2}{3}\right) \end{aligned} \tag{A.29}$$

so that

$$I_1 = \frac{q \exp(-q^2)}{\sqrt{\pi}} \left[\ln\left(\frac{8\gamma\phi_0^2}{3}\right) + \pi \operatorname{erfi}(q) - 2\sqrt{(\pi)} \int_0^q \mathrm{d}x \, \exp(x^2) \operatorname{erfc}(x) \right] \tag{A.30}$$

which is the expression quoted in the text (equation (3.28)), $R(q)$ being the integral term. Another useful form for this integral may be obtained using the formula

$$\pi \operatorname{erfi}(q) - R(q) = S(q) - 2 + \sqrt{(\pi)} q^{-1} \exp(q^2) \operatorname{erf}(q) \tag{A.31}$$

where

$$S(q) = 2 \int_0^1 \frac{p^2 \, \mathrm{d}p}{1-p^2} \{\exp[q^2(1-p^2)] - 1\} = \sum_{n=1}^\infty (2q)^{2n} \frac{(n-1)!}{(2n+1)!}. \tag{A.32}$$

In particular note that (A.31) is of order q^2 when q is small.

We shall now evaluate the spatial coherence function (3.36). We first note that integration of the first term of this equation by parts gives

$$I_1 = \frac{2q}{\pi}\int_0^\infty \mathrm{d}x\, \cos(qx)\exp\left(\frac{-x^2}{4}\right)\left[\mathrm{Ci}\left(\frac{k\xi\chi}{z\sqrt{3}}\right) - \mathrm{Ci}\left(\frac{k\xi\chi x}{(2\sqrt{2})z\phi_0}\right)\right]. \tag{A.33}$$

We have extended the upper limit to infinity as in the derivation of (3.27) of the text and scaled the variable of integration to obtain this formula. Defining $I = I_1\pi/2q$ and differentiating I with respect to q we eventually obtain in close analogy with the derivation of (A.28) above:

$$I(q) = \frac{\pi}{2}\exp(-q^2)\int_0^q \mathrm{d}x\, \exp(x^2)\left[\mathrm{erf}\left(x + \frac{k\xi\chi}{(2\sqrt{2})z\phi_0}\right) + \mathrm{erf}\left(x - \frac{k\xi\chi}{(2\sqrt{2})z\phi_0}\right)\right] + I(0)\exp(-q^2) \tag{A.34}$$

with

$$I(0) = \int_0^\infty \mathrm{d}x\, \exp\left(-\frac{x^2}{4}\right)\left[\mathrm{Ci}\left(\frac{k\xi\chi}{z\sqrt{3}}\right) - \mathrm{Ci}\left(\frac{k\xi\chi x}{(2\sqrt{2})z\phi_0}\right)\right] \tag{A.35}$$

(A.35) may be integrated to give

$$I(0) = \sqrt{(\pi)}\left[\mathrm{Ci}\left(\frac{k\xi\chi}{z\sqrt{3}}\right) + \frac{1}{2}\mathrm{E}_1\left(\frac{k^2\xi^2\chi^2}{8z^2\phi_0^2}\right)\right] \tag{A.36}$$

so that we have, for I_1:

$$I_1 = \frac{q\exp(-q^2)}{\sqrt{\pi}}\left\{2\,\mathrm{Ci}\left(\frac{k\xi\chi}{z\sqrt{3}}\right) + \mathrm{E}_1\left(\frac{k^2\xi^2\chi^2}{8z^2\phi_0^2}\right) + \sqrt{\pi}\int_0^q \mathrm{d}x\, \exp(x^2)\left[\mathrm{erf}\left(x + \frac{k\xi\chi}{(2\sqrt{2})z\phi_0}\right) + \mathrm{erf}\left(x - \frac{k\xi\chi}{(2\sqrt{2})z\phi_0}\right)\right]\right\}. \tag{A.37}$$

The second double integral in (3.36) may be evaluated by noting that the upper limit (x) of the x' integration may be extended to infinity as usual without introducing significant error. Integrating over x' obtains

$$\begin{aligned} I_2 &= \frac{k\xi}{2\phi_0 z\sqrt{(2\pi)}}\int_{\xi/\sqrt{3}}^\infty \mathrm{d}x\left[2\cos\left(\frac{k\chi x}{z}\right)\exp\left(-\frac{k^2\xi^2x^2}{8z^2\phi_0^2}\right) + \exp\left(-\frac{k^2\xi^2}{8z^2\phi_0^2}(x+\chi)^2\right) + \exp\left(-\frac{k^2\xi^2}{8z^2\phi_0^2}(x-\chi)^2\right)\right] \\ &= \exp\left(-\frac{2\phi_0^2\chi^2}{\xi^2}\right)\mathrm{Re}\,\mathrm{erfc}\left(q + \frac{\mathrm{i}k\xi\chi}{(2\sqrt{3})zq}\right) \\ &\quad + \frac{1}{2}\left[\mathrm{erfc}\left(q + \frac{k\xi\chi}{(2\sqrt{2})z\phi_0}\right) + \mathrm{erfc}\left(q - \frac{k\xi\chi}{(2\sqrt{2})z\phi_0}\right)\right]. \end{aligned} \tag{A.38}$$

The spatial coherence function is the sum of (A.37) and (A.38). Note that the integral remaining in (A.37) is only important for large values of q. For small values of q it is of

order q^2. If we retain powers of q up to the first in this limit, we obtain:

$$g^{(2)}(z,\chi)=1+|g^{(1)}(z,\chi)|^2-\frac{2q}{\sqrt{\pi}}\left[\frac{\sin(k\xi\chi/z\sqrt{3})}{(k\xi\chi/z\sqrt{3})}+\exp\left(-\frac{k^2\xi^2\chi^2}{8z^2\phi_0^2}\right)\right]$$
$$+\frac{2q}{\sqrt{\pi}}\left[\mathrm{Ci}\left(\frac{k\xi\chi}{z\sqrt{3}}\right)+\frac{1}{2}\mathrm{E}_1\left(\frac{k^2\xi^2\chi^2}{8z^2\phi_0^2}\right)\right] \tag{A.39}$$

which is formula (3.37) of the text. ($|g^{(1)}(z,\chi)|$ is given by equation (3.21).)

References

Abramowitz M and Stegun I A 1965 *Handbook of Mathematical Functions* (New York: Dover)

Beckmann P and Spizzichino A 1963 *The Scattering of Electromagnetic Waves from Rough Surfaces* (Oxford: Pergamon)

Booker H G, Ratcliffe J A and Shinn D H 1950 *Phil. Trans. R. Soc.* A **242** 579–607

Bowhill S A 1961 *J. Res. NBS* D **65** 275–91

Bramley E N and Young M 1967 *Proc. IEE* **114** 553–6

Briggs J 1963 *Met. Mag.* **92** 69–75

Buckley R 1971 *Aust. J. Phys.* **24** 351–71, 373–96

Cummins H Z and Pike E R (eds) 1974 *Photon Correlation and Light-Beating Spectroscopy* (New York: Plenum)

Dainty J C (ed.) 1975 *Laser Speckle and Related Phenomena: Topics in Applied Physics* vol. 9 (Berlin: Springer)

Erdélyi A 1953 *Higher Transcendental Functions* vol. 2 (New York: McGraw-Hill)

—— 1954 *Tables of Integral Transforms* vol. 1 (New York: McGraw-Hill)

Fried D L 1965 *J. Opt. Soc. Am.* **55** 1427–35

—— 1976 *J. Opt. Soc. Am.* **66** 1150–60

Fujii H and Asakura T 1977 *Appl. Opt.* **16** 180–3

Furuhama Y 1975 *Radio Sci.* **10** 1037–42

Gochelashvily K S and Shishov V I 1975 *J. Opt. Quant. Electron.* **7** 524–36

Goodman J W 1975 *Opt. Commun.* **14** 324–7

Hanbury-Brown R 1968 *A. Rev. Astron. Astrophys.* **6** 13

Jakeman E 1970 *J Phys. A: Gen. Phys.* **3** 201–15

—— 1974 *Photon Correlation and Light-Beating Spectroscopy* eds H Z Cummins and E R Pike (New York: Plenum) pp 75–149

Jakeman E and McWhirter J G 1976 *J. Phys. A.: Math. Gen.* **9** 785–97

Jakeman E, McWhirter J G and Pusey P N 1976 *J. Opt. Soc. Am.* **66** 1175–81

Jakeman E, Oliver C J and Pike E R 1968 *J. Phys. A: Gen. Phys.* **1** 497–9

Jakeman E and Pike E R 1969 *J. Phys. A: Gen. Phys.* **2** 115–25

Jakeman E and Pusey P N 1975 *J. Phys. A: Math. Gen.* **8** 369–91

—— 1976 *IEEE Trans. Antennas Propag.* **AP-24** 806–14

Jakeman E and Welford W T 1977 *Opt. Commun.* **21** 72–9

Marians M 1975 *Radio Sci.* **10** 115–9

Mercier R P 1962 *Proc. Camb. Phil. Soc.* A **58** 382–400

Parry G, Pusey P N, Jakeman E and McWhirter J G 1977 *Opt. Commun.* in the press

Prokhorov A M, Bunkin F V, Gochelashvily K S and Shishov V I 1975 *Proc. IEEE* **63** 790–811

Rice S O 1944 *Bell Syst. Tech. J.* **23** 282

Rumsey V H 1975 *Radio Sci.* **10** 107–14

Salpeter E E 1967 *Astrophys. J.* **147** 433–48

Shishov V I 1971 *Izv. Vuz. Radiofiz.* **14** 85–92

Singleton D G 1970 *J. Atmos. Terrest. Phys.* **32** 187–208

Taylor L S and Infosino C J 1975 *J. Opt. Soc. Am.* **65** 78–84

Whale H A 1973 *J. Atmos. Terrest. Phys.* **35** 263–74

—— 1974 *J. Atmos. Terrest. Phys.* **36** 1045–57

—— 1976 *J. Atmos. Terrest. Phys.* **38** 671–6